AD-A184 681 MILLIMETER-WAVE STUDIES OF MOIST AIR(U) NATIONAL TELECOMMUNICATIONS AND INFORMATION ADMINISTRATION BOULDER CO H J LIEBE 01 JUN 87 ARO-21677 7-GS 1/1

UNCLASSIFIED MIPR-ARO-107-86 F/G 4/1 NL

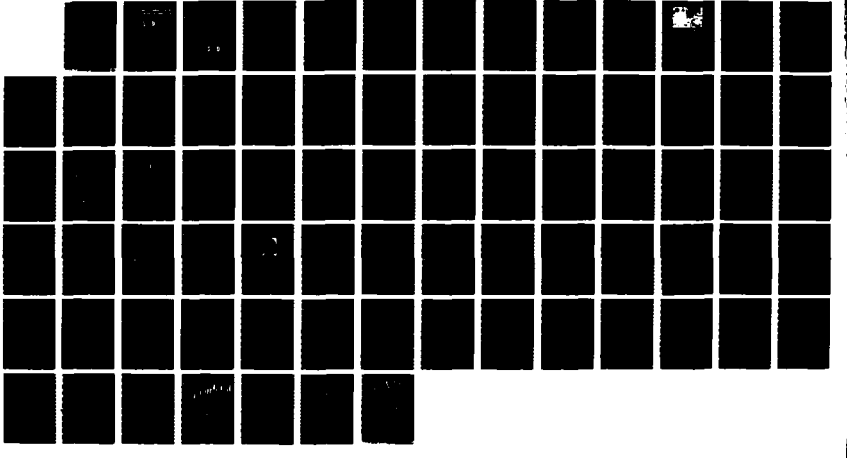

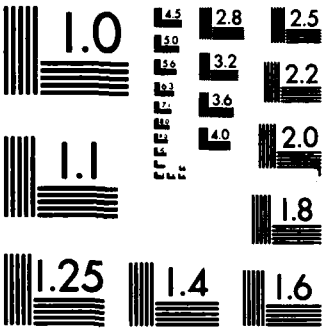

(2)

NATIONAL TELECOMMUNICATIONS AND INFORMATION ADMINISTRATION

MILLIMETER-WAVE STUDIES OF MOIST AIR

-Final Report-

Hans J. Liebe

1 June 1987

U.S. Army Research Office Contract No. 107-86

Institute for Telecommunication Sciences
Boulder, Colorado 80303

(2)

MILLIMETER-WAVE STUDIES OF MOIST AIR

-Final Report-

Hans J. Liebe

1 June 1987

U.S. Army Research Office Contract No. 107-86

APPROVED FOR PUBLIC RELEASE;
DISTRIBUTION UNLIMITED.

UNCLASSIFIED
SECURITY CLASSIFICATION OF THIS PAGE

ADA184681

REPORT DOCUMENTATION PAGE

1a. REPORT SECURITY CLASSIFICATION Unclassified	1b. RESTRICTIVE MARKINGS
2a. SECURITY CLASSIFICATION AUTHORITY	3. DISTRIBUTION/AVAILABILITY OF REPORT Approved for public release; distribution unlimited.
2b. DECLASSIFICATION/DOWNGRADING SCHEDULE	
4. PERFORMING ORGANIZATION REPORT NUMBER(S)	5. MONITORING ORGANIZATION REPORT NUMBER(S)
6a. NAME OF PERFORMING ORGANIZATION Nat'l. Telecomm. & Info. Admin Inst. for Telecomm. Sciences 6b. OFFICE SYMBOL (If applicable) NTIA/ITS	7a. NAME OF MONITORING ORGANIZATION U. S. Army Research Office
6c. ADDRESS (City, State, and ZIP Code) 325 Broadway Boulder, CO 80303 3328	7b. ADDRESS (City, State, and ZIP Code) P. O. Box 12211 Research Triangle Park, NC 27709-2211
8a. NAME OF FUNDING/SPONSORING ORGANIZATION U. S. Army Research Office 8b. OFFICE SYMBOL (If applicable) ARO-GS	9. PROCUREMENT INSTRUMENT IDENTIFICATION NUMBER MPIR ARO 107-86
8c. ADDRESS (City, State, and ZIP Code) P. O. Box 12211 Research Triangle Park, NC 27709-2211	10. SOURCE OF FUNDING NUMBERS PROGRAM ELEMENT NO. / PROJECT NO. / TASK NO. / WORK UNIT ACCESSION NO.

11. TITLE (Include Security Classification)
Millimeter-Wave Studies of Moist Air (Unclassified)

12. PERSONAL AUTHOR(S)
Hans J. Liebe

13a. TYPE OF REPORT	13b. TIME COVERED	14. DATE OF REPORT (Year, Month, Day)	15. PAGE COUNT
Final Report	FROM 10/84 TO 3/87	1987 June 01	70

16. SUPPLEMENTARY NOTATION
The view, opinions and/or findings contained in this report are those of the author(s) and should not be construed as an official Department of the Army position, policy, or decision, unless so designated by other documentation.

17. COSATI CODES			18. SUBJECT TERMS (Continue on reverse if necessary and identify by block number)
FIELD	GROUP	SUB-GROUP	

19. ABSTRACT (Continue on reverse if necessary and identify by block number)

Accurate laboratory measurement of attenuation rates α_x over a range from 0.1 to 10 dB/km at 138 GHz for water vapor (H_2O) and its mixtures with air, nitrogen (N_2), oxygen (O_2), and Argon (Ar) have been performed over a temperature range from 8 to 43°C, relative humidities up to 95% RH, and total pressures reaching 1.5 atm. A computer-controlled resonance spectrometer was employed. The results are interpreted in terms of underlying absorption mechanisms. Broadening efficiencies m measured for mixtures $H_2O + N_2$, $H_2O + O_2$, + Ar agree among themselves with those measured within cores of the 22 and 183 GHz H_2O absorption lines. The m-factors are applied to predict what share α_ℓ of the total α_x comes from the complete pressure-broadened H_2O spectrum. The results indicate that a substantial amount of the self-broadening term proportional to the square of vapor pressure is left unaccounted. The negative temperature coefficient of the excess absorption is consistent with a dimer $(H_2O)_2$ model. A spectroscopic data base limited to 30 local H_2O lines (centered below 1 THz) contributes about 1/3 to α_ℓ at 138 GHz. An empirical formulation of the experimental findings is

20. DISTRIBUTION/AVAILABILITY OF ABSTRACT	21. ABSTRACT SECURITY CLASSIFICATION
☒ UNCLASSIFIED/UNLIMITED ☐ SAME AS RPT. ☐ DTIC USERS	Unclassified
22a. NAME OF RESPONSIBLE INDIVIDUAL	22b. TELEPHONE (Include Area Code) / 22c. OFFICE SYMBOL

DD FORM 1473, 84 MAR — 83 APR edition may be used until exhausted. All other editions are obsolete.

SECURITY CLASSIFICATION OF THIS PAGE
UNCLASSIFIED

19. continued:

incorporated into the parametric propagation model MPM that utilizes a local (30x H_2O, 48 x x O_2) line base to address frequencies up to 1000 GHz. Predictions of moist air attenuation and delay rates by means of the revised MPM program generally compare favorably with reported (10 - 430 GHz) data from both field and laboratory experiments, except for subfreezing transmission data in the 190 to 260 GHz range.

TABLE OF CONTENTS

1. INTRODUCTION

The near-millimeter region of the spectrum (NMMW: 0.1-1 THz) is an active area for research. Possible applications lie in short-range communications, radar, radiometry, and radio astronomy. Atmospheric effects of transmission and emission dominate performance simulations and the complex refractivity N provides a measure of the interactions between radiation and the atmospheric propagation medium. A reliable N-model allows calculation of frequency-dependent rates for delay (real part) and attenuation (imaginary part) based on measurable meteorological variables. Dry air and atmospheric water vapor are major millimeter-wave absorbers; so are suspended droplets (haze, fog, cloud) and precipitating water drops that emanate from the vapor phase. Laboratory research and analytical studies have been conducted with the primary purpose of understanding NMMW attenuation (α, db/km)^c and delay(β, ps/km)^c rates. Emphasis was placed on the fundamental concepts that support an α/β formulation.

Refractivity N for moist air can be obtained, in principle, by a line-by-line summation over all molecular absorption lines. In practice, various degrees of approximations are employed to reduce labor and computer time required, since the number of contributing spectral lines by the dominant absorbers (water vapor and oxygen) and by various trace gases (e.g., O_3) exceeds 10,000. A practical NMMW model, indexed MPM, consists of local H_2O (30x) and O_2 (48x) lines below 1 THz and an approximation to the contributions by H_2O lines above 1 THz [3], [6], [8], [9], [Appendix].

The experiments have been performed at 138 GHz to measure absolute attenuation rates by dry air, moist air, water vapor, and water-vapor mixtures with nitrogen (N_2), oxygen (O_2), and argon (Ar) at temperatures between 8 and 43°C, total pressures up to 1 atm and higher, and relative humidities up to 95 percent. The experimentally observed absorption is not described by standard line shape models. Such failure reveals difficulties in modeling frequency, temperature and pressure dependencies for moist air attenuation. An unexplained excess is identified for which the name "water-vapor continuum" was coined since it appears to increase smoothly with frequency within the NMMW range.

Experimental studies inspired model formulations along practical lines. The MPM program is a user-friendly, PC-operated code that generates numerical values of $\alpha(f)$ and $\beta(f)$ for frequencies f up to 1000 GHz. Input parameters are five measurable atmospheric quantities: barometric pressure P, ambient temperature T, relative humidity RH, suspended droplet water content w, and rainfall rate R. Controlled laboratory measurements were limited to moist air studies (P, T, RH), and the data obtained at 138 GHz are reasonably complete and accurate to assess water vapor pressure and temperature dependencies for the water-vapor continuum. Both variabilities point to the distinct possibility of an absorption mechanism related to water vapor but not accounted for by molecular theory of H_2O.

This report is organized in three parts. The first part (Section 2) gives details of the experimental setup, its achieved performance, and a summary of reduced data. After many improvements, a detection sensitivity of $\alpha_{min} \approx 0.05$ dB/km or $1.2 \times 10^{-7} cm^{-1}$ was realized. In the second part (Section 3), results from the laboratory experiments are applied (a) to calibrate the MPM program with an empirical continuum term, (b) to demonstrate the parametric flexibililty of the code (i.e.; f, RH, and P can be selected as variables), and (c) to conjecture on the physical basis of a NMMW water vapor continuum that is defined by the limited H_2O line base of MPM. A final section 4 contains examples of recently reported data from laboratory and field experiments on water vapor absorption (10-430 GHz) and their comparison with MPM predictions. Overall agreement is good, particularly in atmospheric transmission windows.

2. LABORATORY STUDIES OF MOIST AIR ABSORPTION AT 138 GHZ

Controlled experiments that simulate atmospheric conditions provide test cases for studying specific contributions to N in isolation. Assessments of basic physical principles underlying the attenuation rate α are difficult to make from measurements in the actual atmosphere. The objective of this study was to measure water vapor continuum absorption. A test frequency of 138 GHz was selected because of its remoteness from local H_2O lines. The expected window attenuation falls in the range 0.1 to 5 dB/km and the required detection sensitivity calls for a long (>0.1 km) effective path length, which can be attained with a resonant absorption cell.

The response curve A(f) of an isolated, high Q-value resonance is detected with a power (square-law) detector. Both, the peak value a_0 at center frequency f_R and the bandwidth b_0 spread over a range $f_R \pm b_0/2$ at the level $a_0/2$ might be used to detect the relative attenuation,

$$\alpha_r = 8.686(\sqrt{a_0/a} - 1) = 8.686(b/b_0 - 1) \quad \text{dB}, \qquad (1)$$

of an absorbing gas, that changes the corresponding quantities to a and b when introduced into the resonator. Around 138 GHz it is possible to design a compact (20 cm mirror spacing) Fabry-Perot resonator with a loaded Q-value on the order of 4×10^5, that defines ($Q = f_R/b_0$) a resonance bandwidth of $b_0 \simeq 350$ kHz.

A crucial question to be resolved is if amplitude (a_0/a) or frequency (b/b_0) detection schemes provide the optimum sensitivity for the spectrometer. After exhaustive testing it was found that digital averaging of A(f), displayed over a frequency span $\Delta f_M = f_R \pm 6b_0$ was capable of resolving $a_0/a \simeq 1.002$ (512 pts) - but only $b/b_0 \simeq 1.015$ with 1024 pts . Amplitude peak-value detection provided optimum sensitivity for absorption studies. The frequency span Δf_M is needed to establish the baseline A(f) = 0 of the resonance response. In addition, a detection at f_R eliminates corrections for dispersive distortions of A(f) [21].

Absolute calibration of absorption is accomplished by defining an equivalent path length (b_0 in kHz),

$$L_E = 47.71/b_0 \quad \text{km}, \qquad (2)$$

for the resonance spectrometer operating at f_R. From (1) and (2) follows that the absolute power attenuation rate of an absorbing gas is given by

$$\alpha = 0.1820 b_o (\sqrt{a_o/a} - 1) \quad \text{dB/km.} \qquad (3)$$

If the assumptions made, so far, can be brought to fruition, then the projected detection sensitivity ($a_o/a = 1.002$, $b_o = 350$ kHz) is $\alpha_{min} = 0.064$ dB/km, which is adequate for the planned water vapor studies.

2.1 Experimental Arrangement

The measuring system consists of the millimeter wave resonance spectrometer and a humidity simulator. An insulated box contains a high-vacuum stainless steel vessel which houses a temperature-controlled mini-lake (10 cm across) and the resonator. Temperatures are controlled to better than 1/100 of a degree Celsius; pressure ranges over seven orders of magnitude (10^2 to 10^{-5} kPa); and relative humidity is varied between 0 and 99.5 percent.

Schematical diagrams of physical and electronic (Figure 1) arrangements convey an overview of the experiment. A temperature-controlled water reservoir serves as the vapor source. Electropolished stainless steel was used exclusively as construction material. Various hydrophobic coatings were studied as possible means for neutralizing the absorption/desorption cycle of surfaces exposed to water vapor [1], but were abandoned in favor of slightly heating the mirrors of the resonator. Four fast-responding ($\tau < 1$s) temperature sensors inside the cell diagnose any disturbance of the gas condition. Data acquisition was computer controlled.

The resonator inside a vacuum chamber (Figure 1c) is the heart of the absorption spectrometer. A key-word summary of its specifications reads as follows: Fabry-Perot reflection-type, semi-confocal arrangement, 10 cm mirror diameter, mirror heating: 1°C/0.3 W; Fresnel number: 6; coupling factor $k = 0.0550$, coupling hole: circular, 0.65 mm diameter, 0.075 mm double Mylar vacuum/pressure seal; resonance frequency, selected for optimum performance of the available klystron, $f_R = 137.80$ GHz, stability $\Delta f/f_R = 1.1 \times 10^{-6}$/°C temperature compensated and insensitive to pressure loads from 0 to 2 atm; resonance bandwidth: $b_o = 334$ kHz yielding an effective path length, $L_E = 0.141$ km (Eq. 2); *mirror spacing:* $x_R = 182\ \lambda/2 = 198.0$ mm; micrometer

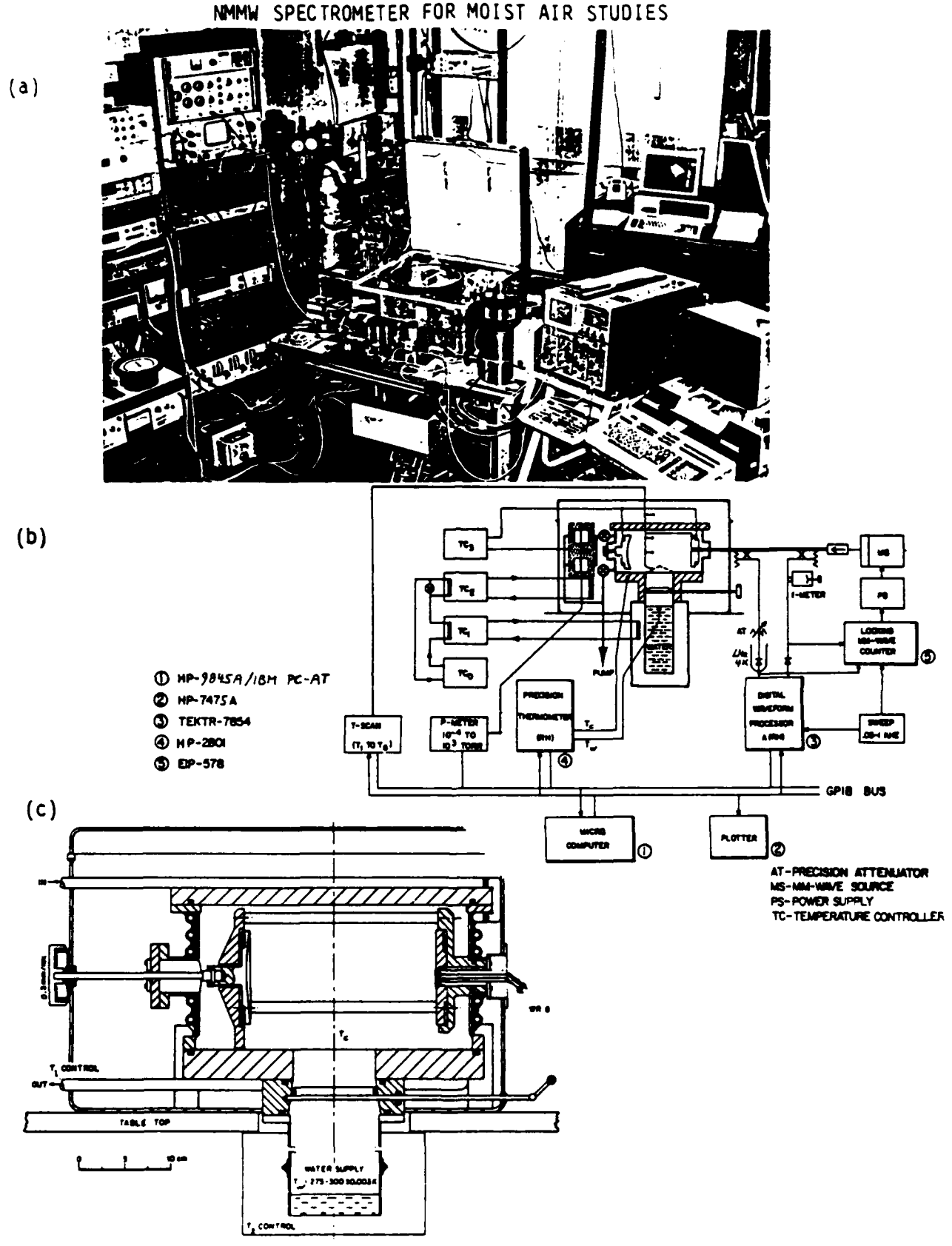

Figure 1. The high-humidity wave spectrometer: (a) photographic view, (b) schematic, (c) cell design.

tuning: 0.3175 mm/rev = 2500 SU/rev with a resolution, Δx_R = 0.127 μm/SU, which converts into a frequency change,

$$\Delta f_R = -f_R(\Delta x/x)_R = -88.4 \text{ kHz/SU}. \qquad (4)$$

Over a 2.5 cm tuning range of the micrometer, the resonance at x_R was the "best" out of 52 choices with respect to other-mode interferences and Q-values.

The detector of the resonance pulse A(t) was an InSb bolometer, cooled to 4.2 K-LHe, and connected by a WR-12 waveguide mount. The maximum voltage output of the preamplifier was 10 V. A power-linear response of 4.2 V/mW was measured up to 1.0 V. With a 50 kHz detection bandwidth, the noise power was about 5 nW. The bolometer bias (92 mV) served as cryogenic thermometer (T_D).

The power source was a 138 GHz klystron (20 mW) that was frequency-modulated by a sawtooth voltage generator to provide frequency-to-time domain conversion. The modulation frequency was exactly 500 Hz derived from a 10 MHz frequency standard. The linear sawtooth ramp was gated at exactly 1925 μs, the fly-back time took only 2 μs, which eliminated A(t) from the retrace. The modulation sensitivity of the klystron was determined accurately to be 12.56 MHz/V by using the resonance peak a_0 as frequency marker, mechanically tuned to the end points of the ramp and checked for linearity over a modulation voltage range from 0.500 to 3.000 V. The tuning uncertainty of 0.5 SU introduced about 0.5 percent error in the frequency-to-voltage conversion factor (12.56 MHz/V).

The reference power $a_0 = k \cdot a_K$ for (1) was measured by periodically (30s) switching on computer command to a 36 V modulation voltage, which displayed the power mode $A_K(t)$ with a peak value, a_K = 909 mV and a bandwidth, b_K = 186 MHz. This feature provided an automatic calibration of α_r (1) when the power level changed during a data run (e.g., refractive-tuning reduces f_R and the peak value a_K can change when the klystron is readjusted).

An electronic lock-on circuit kept the rsonance f_R centered with[illegible] time frame; that is, the klystron center frequency $f_K(a_K)$ was prevented from drifting with reference to f_R. A flat baseline A(t) = 0 was established by adjusting f_K in such a way that two adjacent A(t) frames were displayed on a control scope and balanced. The reflected resonance signal A(t) could be

eliminated by injecting a steel rod into the resonance volume. This measure provided baseline reference data in the "low" (0.36 V) and more accurate peak readings a_K in the "high" (36 V) mode of the modulator.

The waveform processor for A(t) was a digital storage oscilloscope, synchronized with the sawtooth modulator and capable of resolving 512/1024 pts per 2000 μs. Operational resolution was typically 3.91 μs/pt. The modulator voltage for A(t)-detection was 0.360 V resulting in a frequency resolution of 9.2 kHz/pt, which is an improvement over (4). Extensive averaging of the repetitive waveforms A(t) and $A_K(t)$ up to 200 times was performed in real time to improve the S/N of the a and b results.

For a measurement of the resonance bandwidth b_o, the digitizing increments were doubled (1024 pts) and the modulation voltage was varied in the 0.150 to 0.400 V range, allowing the resolution uncertainty to be reduced to ±5 kHz. The resulting error in an absolute calibration of α (3) was less than 3 percent.

The computer control-program for the spectrometer was designed to be flexible in order to allow changes in data collection procedures. The program is written in BASIC with about 500 lines of code to control the readings of eight temperatures, two pressures, and a/b values from the waveform processor and store the data on a magnetic medium for future processing. The program is time controlled. The fastest acquisition time for a complete measurement cycle was 30 seconds.

Measurements begin by starting the internal program of the waveform-processor, which does 100 averages on the output A(t) from the InSb detector. Since averaging takes about 14 seconds, the computer program continues data recovery from the temperature sensors which measure chamber (T_c), water bath (T_w), room (T_r), gas ($T_{1,2,3}$), mirror (T_m) temperatures, and from the total pressure meter (P). By this time the oscilloscope is nearly ready with its data so the computer program returns to wait for the final steps in the scope program. After the scope completes the 100 averages on A(t) it normalizes the trace to remove any baseline slope, then stores the waveform. Next, an auxiliary output from the scope switches the sweep generator voltage from low (0.36 V) to high (36 V). The scope input changes to the power envelope of the klystron with the lock-on disabled. The scope program performs 50 averages on the power curve and stores the waveform A_K. The next computer step is to call for the a/b and a_k/b_k values of the stored waveforms.

All of the measured data are temporarily stored in computer memory and permanently stored along with time-of-day on magnetic tape or disk storage for safe keeping and later recovery and processing.

Real time data were plotted on the CRT of the computer to follow the progress of an experiment. The selection of what was displayed is part of the program configuration. Two typical examples of 1-hour operating periods are shown in Figure 2. Figure 2a demonstrates the automatic calibration to α_r = 0 dB for input power variations of 1 dB. The reference power trace a_K was reduced by a factor 0.05 for display, but the correct coupling factor k = 0.0550 was applied for the relative attenuation trace (1) $\alpha_r = 8.686\ (\sqrt{k \cdot a_K / a} - 1) = 0$ dB. Each 1-hour frame represents an average of 8.96×10^6 actually acquired data. Detection sensitivity and long-term stability are displayed in Figure 2b.

Program configuration is stored in a separate file on disk. An auto-start function is available for studies that are conducted unattended. In the event of a power failure the program will automatically re-start.

Post-processing of data repeats the calibrated signal correction as done in the real-time mode. Scatter plots of α_r are made versus pressure in a point-mode.

2.2 Moist Air Attenuation Measurements

The objective of the experiments was to perform pressure scans of the attenuation rate α due to water vapor absorption in moist air. An extensive series of controlled measurements was performed at 137.8 GHz to determine $\alpha(P = e+p)$. Over 2000 individual data points $\alpha(T, e, p)$ were taken covering the following range of parameters:

temperature	T = 316 to 282 K;
vapor pressure	e = 0 to e_1 (RH > 95%); and
total pressure	P = e_1 + p, where p = 0 to 1200 torr (capacitance manometer), p = 0 to 3 atm (aneriod manometer)*.

Maximum vapor pressure e_1 was determined by the temperature T_W of the water reservoir [see (2)-A].

*Experimental pressure scale is measured in torr, the prediction model MPM uses the pressure unit 1 kPa = 10 mb = 7.5006 torr.

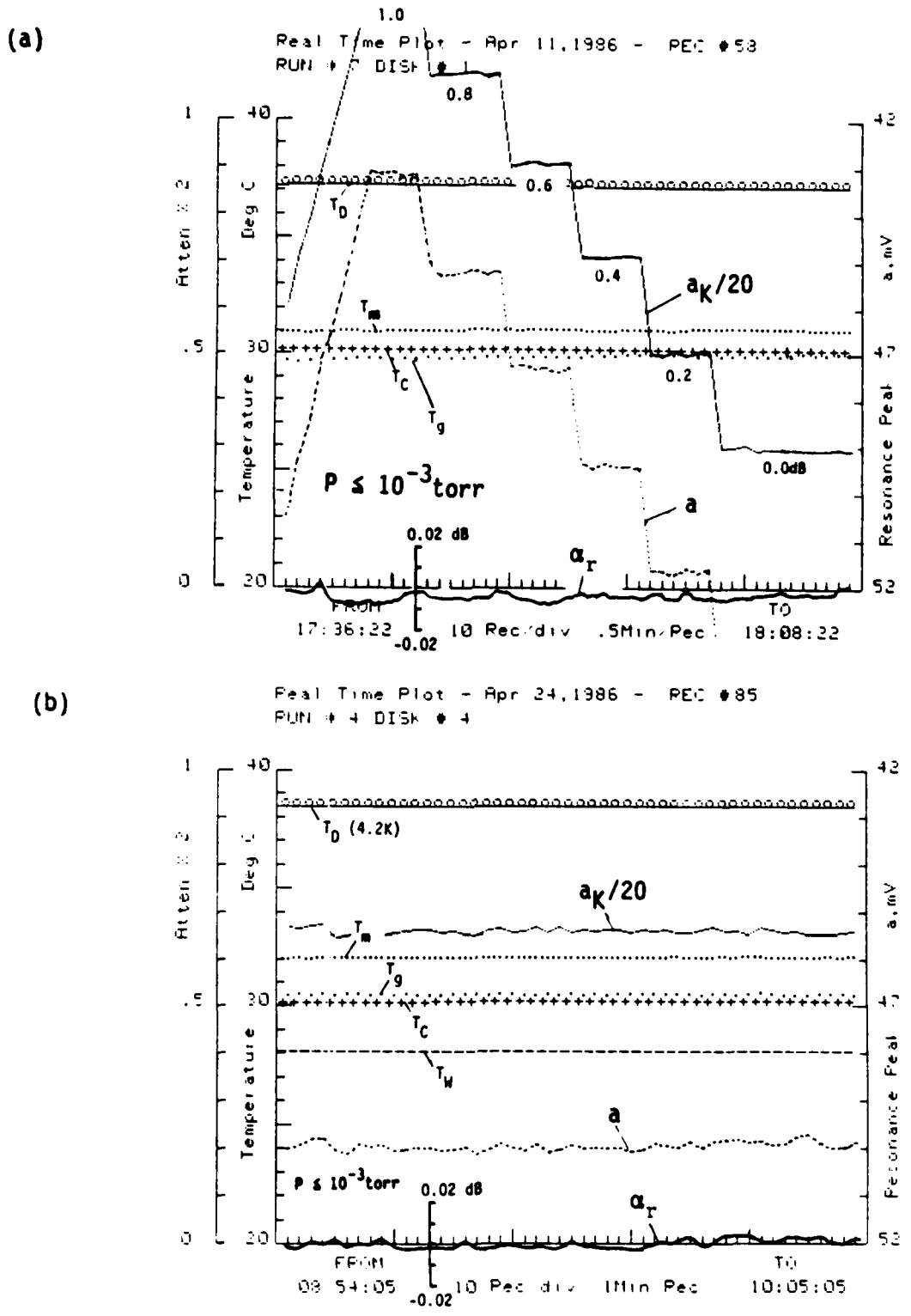

Figure 2. Mm-wave spectrometer operational data (5 temperatures T; peak values of reference and reflected signals a_K, and a; and relative attenuation α_r) for a one-hour measurement period with an evacuated cell (f_R = 137.8 GHz): (a) automatic calibration to α_r = 0 dB for changes, Δa_K = 0-1 dB; (b) detection stability and sensitivity (α_{min} = 0.006/0.13 ≤ 0.05 dB/km.)

With the spectrometer performance optimized at P = 0 (see Figure 2b), an additional set of problems appeared when the gas pressure was varied. Introducing and removing gas from an enclosure changes the temperature T_g of a sample (Figure 3). Only pressure scan rates below ± 100 torr/min ensured quasi-static gas conditions, $T_g = T_C$. Typically, the pressure was varied in steps. While the gas settled, the klystron frequency f_K was retuned to balance the base-line of A(t).

Working with water vapor often brought disappointing results with respect to reproductibility. One source was the "piston" effect where local compression condenses part of the vapor; another error source was the slow diffusion-mixing of water vapor with stagnant air. We calculated the diffusion time constant for vapor molecules to travel 30 cm inside the cell against 1 atm of dry air to be:

T (K)	315	300	285
τ_D (min)	5.4	6.0	6.7 .

It takes a period longer than $5 \cdot \tau_D$ for a homogeneous moist air mixture $P = e_1 + p$ to develop. A measurement of a(P) shown in Figure 4a indicates even longer time periods. Water pressure $e_1(T_W)$ settled with no delay when the H_2O-valve was opened. Dry air injection first reduced e_1 (piston effect) and then it took up to 1 hour to obtain a stable value $a(e_1+p)$. Mixing was accelerated to less than 5 minutes by installing a fan, driven by a magnetically-coupled rotary feed-through.

One other effect was observed when dealing with moist air inside a vessel: reducing the total pressure P caused the water vapor to condense by decompression cooling. Even with the water vapor supply fully exposed to the air mixture, it took a long time (20 min) to reestablish the initial vapor pressure e_1 as indicated by $\alpha_r(P)$ in Figure 4b (the mixing fan was off).

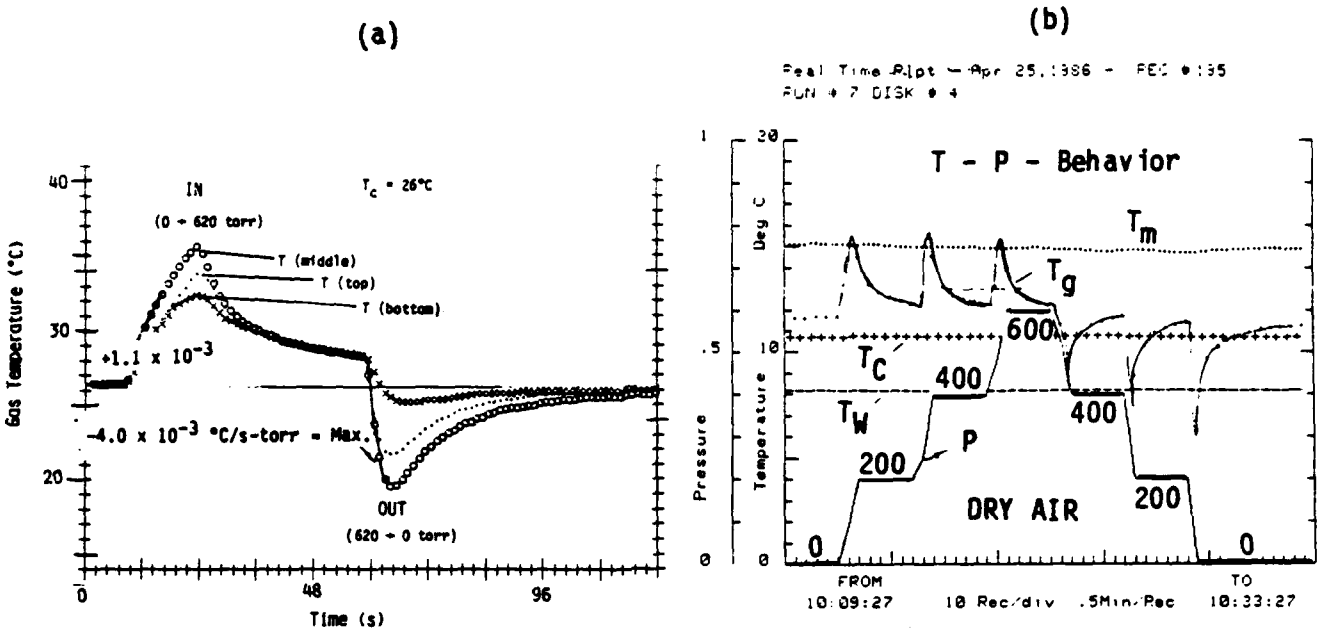

Figure 3. Temperature responses inside the spectrometer cell:
(a) time-response test of gas temperature (T_g) sensors,
(b) temperature-vs.-pressure behavior for a typical dry air case.

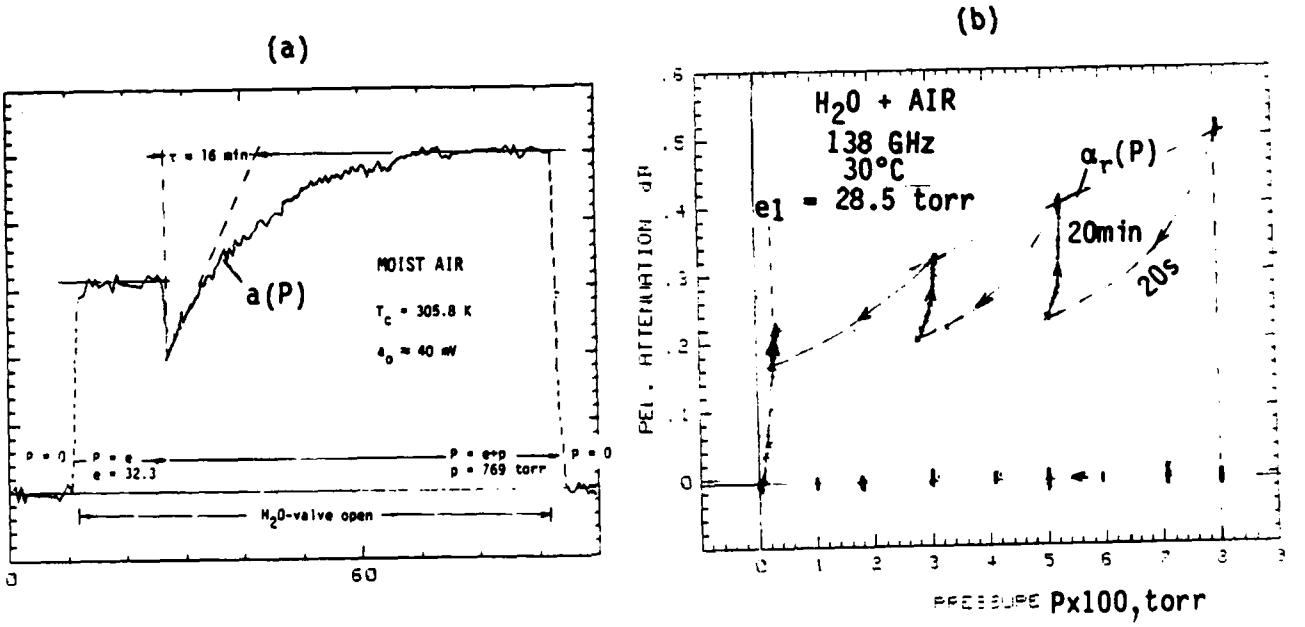

Figure 4. Mixing effects of H_2O + AIR from time series of 138 GHz attenuation:
(a) piston effect and diffusion mixing;
(b) decompression condensation during pump-down over open vapor source.

2.3 Water Vapor and Moist Air Attenuation Results

Moist air attenuation α at a frequency f that falls within the millimeter-wave window range centered at 140 GHz, can be expressed by [14], [17]

$$\alpha = k_s(T)\ e^2 + k_f(T)\ ep + k_d(T)\ p^2 \quad \text{dB/km}, \tag{5}$$

where e and p in kPa are partial pressures of water vapor and dry air, respectively. Pressure-broadening theory of the H_2O rotational spectrum predicts ($e > 0.01$) a fixed ratio m between air-(ep) and self-(e^2) broadening; i.e.,

$$m = k_f/k_s. \tag{6}$$

An extensive series of controlled laboratory measurements was performed at 137.8 GHz to determine the k-coefficients of (5) and (6). Table I is a summary of over 2500 individual data points $\alpha(T, e, p)$.

At $T = 303$ K, the foreign-gas broadener AIR (p) was replaced by its principal constituents N_2, O_2, and Ar. These results are summarized in Table II. The broadening efficiency m is useful to explain H_2O absorption processes that support (5) since $\alpha = k_s e\ (e+mp)$. Pure oxygen (O_2) measurements for pressures up to 2.4 atm against Ar as the "loss-free" reference provided an estimate of k_d when multiplying the result by 0.21.

Data of Table I were further reduced to a reference temperature $T_o = 300$ K or inverse T-parameter, $\theta = 300/T$. The temperature dependence of the $k_{s,f,d}$ coefficients was fitted to a power law,

$$k(T) = k\theta^x \quad \text{dB/km-kPa}^2. \tag{7}$$

The results for moist air attenuation at 137.8 GHz, when expressed by (5) to (7), led to

TABLE I.

Comparison Between Measured (X) and Model-predicted (M=MPM, see Section 3) Coefficients $k_{s,f}$ of (5). Experimental Conditions: f=137.8 GHz, T=282-316 K, $P=e_1 + p$, p=0-110 kPa.

	T	e_1(RH)	Moist Air k_s	Moist Air k_f	Moist Air m	Dry Air k_d
	K	kPa	dB/km-kPa^2 x10^{-2}		x10^{-2}	dB/km-kPa^2 x10^{-6}
X	315.5	7.49 (90%RH)	8.01	0.485	6.06	-
M			7.85	0.481	6.13	1.93
X	305.9	4.45 (90%RH)	10.9	0.540	4.95	-
M			10.81	0.530	4.90	2.10
X	303.2	3.80 (90%RH)	12.0	0.558	4.65	2.2
M			11.84	0.545	4.60	2.11
X	296.1	2.51 (90%RH)	15.0	0.59	3.9	-
M			15.08	0.589	3.91	2.29
X	286.7	1.39 (90%RH)	21.0	0.65	3.1	-
M			21.22	0.649	3.06	2.46
X	28 .8	1.05 (94%RH)	25.7	0.68	2.65	-
M			25.49	0.687	2.70	2.64

$$k_s(T) = 0.133(4)\theta^{10.3(3)},$$
$$k_f(T) = 5.68(5)10^{-3}\theta^{3.0(4)}, \qquad (8)$$
$$k_d(T) = 2.2(5)10^{-6}\theta^{2.8},$$

and

$$m = 0.0427/\theta^{7.3}.$$

Digits in parenthesis give the standard deviation from the mean in terms of the final listed digits. Typical examples of data plots $\alpha_r(e)$ and $\alpha_r(e_1 + p)$ are exhibited in Figure 5. All experimental results supported the formulation in equation (5). Model predictions of the experimental data are given in Figure 14 (Section 3.4).

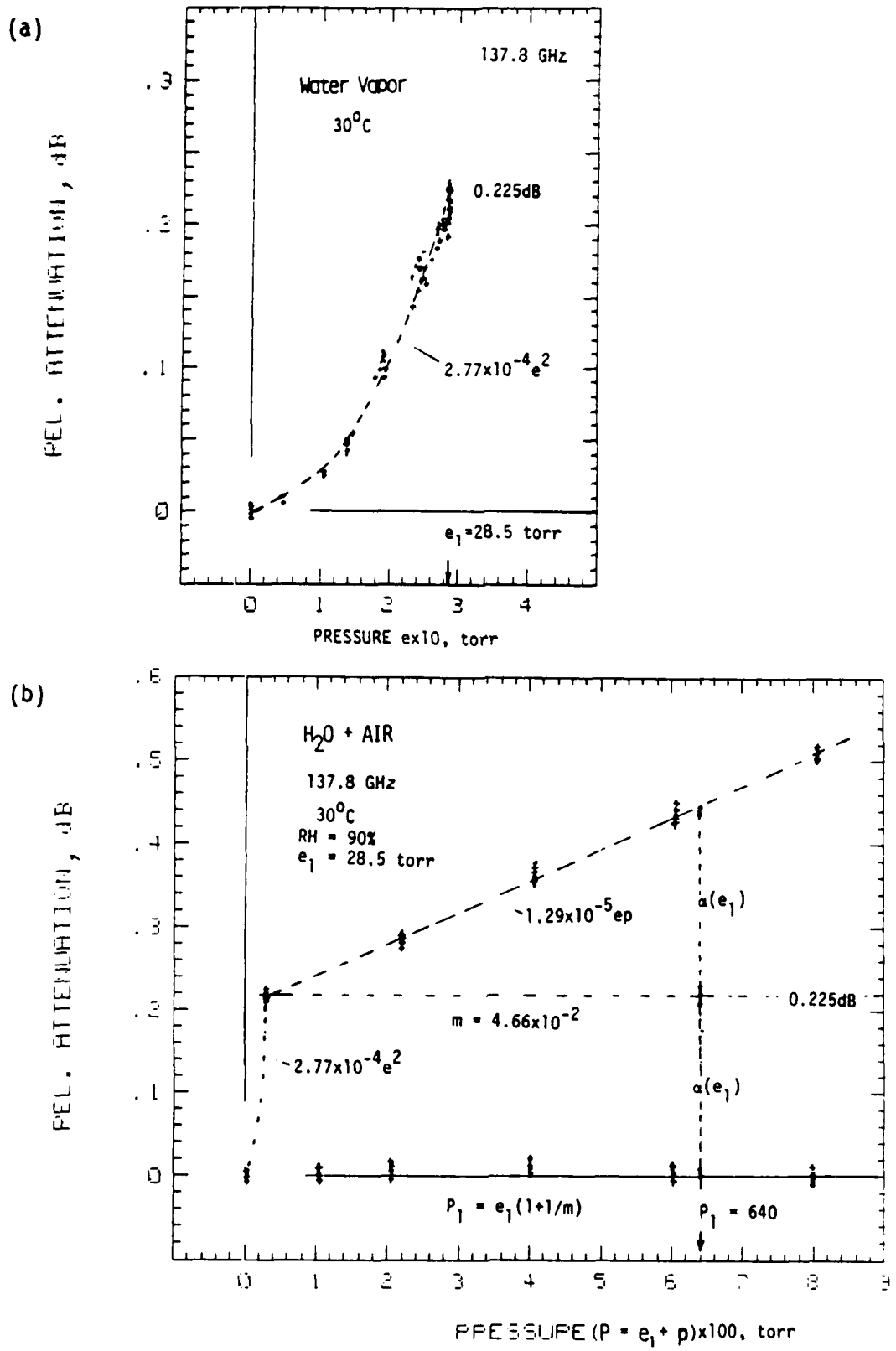

Figure 5.

Typical raw data plots of relative attenuation $\alpha(P)$ for pressure scans at 137.8 GHz introducing (a) water vapor, $P = e$; and (b) air, $P = e_1 + p$.

TABLE II.

Attenuation Measurements of Water-vapor/Air-constituent Mixtures (f=137.8 GHz, T=303 K, e_1=3.80 and p=0-100 kPa) Expressed with k_X-Coefficients of (5), and Corresponding Broadening Efficiencies m_X (6). Also given are Line-core Measurements m_L and their Resultant Predictions m_1 and k_1 for 138 GHz.

	FAR WING (303K)				LINE CORE (300K)		
	k_X	k_1	m_X	m_1	m_L		
f(GHz)	137.8		137.8		22.2	183.3	
Species	dB/km-kPa^2 x10^{-2}		x10^{-2}		[13]	[13]	[15]
					x10^{-2}		
H_2O	12.0	2.55	100	100	100	100	100
AIR	0.558		4.65	21.9*	20.8	22.7	$22.1(\theta^{-0.6})$
N_2	0.627		5.23	24.6	22.8	24.9	
O_2	0.322		2.68	12.6	14.0	14.3	
Ar	0.222		1.85	8.7	11.4	10.3	
	Linewidth (MHz/kPa)				135.0	143.0	$151.9(\theta^{1.1})$

*Reference (line-core average)

3. ATMOSPHERIC PROPAGATION MODEL MPM
(see Appendix for Details)

Dry air and atmospheric water vapor are major millimeter-wave absorbers; so are suspended droplets (haze, fog, cloud) and precipitating water drops that emanate from the vapor phase. A practical model (designated program code: MPM) was formulated that simulates the refractive index $\underline{n} = n' - jn''$ of the atmospheric propagation medium for frequencies up to 1000 GHz [3], [8], [9]. Since the interaction with a neutral atmosphere is relatively weak, the refractive index is converted into a refractivity in units of parts per million,

$$\underline{N} = (\underline{n} - 1)\ 10^6 \quad \text{ppm.}$$

3.1 Features of the Program

A user-friendly parametric program was developed that calculates the values of the complex refractivity $\underline{N}$ for atmospheric conditions as a function of the variables f, P, T, RH, w_A (A/B/C/D), w, and R, as listed in tne scheme below:

Variable	Symbol	Validity Range	Medium
frequency	f	≤ 1000 GHz	
barometric pressure	P	120-0 kPa	Moist
temperature	T	- 50- + 50°C	Air
relative humidity	RH	0-100%	
haze model: code A, B, C, D (or combinations thereof) plus hygroscopic aerosol reference concentration	w_A(80%RH)	RH=80-99.9% 0-1 mg/m^3	Haze
suspended water droplet concentration	w(100%RH)	0-10 g/m^3	Fog, Cloud
rain fall rate	R	0-200 mm/h	Rain

The output of MPM are three radio path-specific quantities,

attenuation	$\alpha(f)$	dB/km,
and		
refractive delay	β_o	ns/km,
dispersive delay	$\beta(f)$	ps/km.

The height range 30 to 100 km is treated approximately excluding the detailed O_2-Zeeman effect and trace gas spectra (e.g., O_3, CO, N_2O, etc.). Program MPM is written with extensive comments to run on IBM-XT/AT + 8087 Coprocessor, or equivalent, microcomputers [9].

Extensive revisions of the MPM code have been made over the last year. The newest version is described in the Appendix. Details include (a) a revised set of overlap coefficients a_5 [(12)-A] in the dry air line table for the 60 GHz oxygen band based on a molecular fitting scheme reported by Rozenkranz [23]; (b) a relative humidity-driven growth model for hygroscopic aersol addressing haze conditions for RH = 90 to 99.9% [(3)-A]; (c) a new double-Debye model describing the complex permittivity $\underline{\varepsilon}(f,T)$ of water for f = 0 - 1000 GHz, T = -10 to 30°C [(17)-A]; and (d) an improved fog/cloud model that includes a dispersive delay term [(16)-A].

3.2 MPM Calibration

The experimental result (5), (8) at 138 GHz contains foremost contributions from water vapor continuum absorption. Equation (5) was used to "calibrate" the program MPM by enforcing the agreement between experimental and predicted data. The resultant continuum, assuming an f^2 dependence, is defined by (see (14a) of [3])

$$\alpha_c = 0.1820\ f\ N''_e(f), \tag{9}$$

where the imaginary part of refractivity $\underline{N}$ is given by (see Table III)

$$N''_e = f(3.57\ e^2\theta^{10.5} + 0.113\ e\ p\ \theta^3)10^{-5} \tag{10}$$

and f is in GHz. The comparison in Table I shows that at 138 GHz, within experimental uncertainties, a good fit was obtained.

In addition to (10), new width data [15] for the 183 GHz H_2O line (b_3 listed in Table 1 of [3] was increased by 11.6%) were used to update the MPM program; also, b_3 parameters of the 325 and 380 GHz H_2O lines were increased by 10 percent. Other MPM modifications were a change in the nonresonant line width γ_o of dry air from 5.6×10^{-3} to 4.8×10^{-3} [23], the elimination of the roll-off term $1/[1 + (f/60)^2]$ (see equation 13 in [3]), and the imposing of a high frequency cut-off $F''(f) = 0$ for $f \geq \nu_o + 40\gamma$ [22].

3.3 Interpretation of H_2O Continuum Absorption

Since MPM employs a limited ($\leq$ 1 THz) H_2O line base, it is of interest to find out which share of k_s and k_f (8) can be attributed to far-wing behavior of the rotational H_2O spectrum extending beyond 1 THz [7], [14]. Results in Table II indicate broadening efficiency ratios η at 138 GHz; e.g.,

$$\eta = m(H_2O + N_2)/m(H_2O + Ar), \tag{11}$$

which are similar to those observed at cores of the 22 and 183 GHz lines. Consequently, k_f can be interpreted as a foreign-gas broadening effect whereby MPM lines account for about 30 percent of the rotational H_2O spectrum. Table III lists the assessment at 300 K ($\theta = 1$). When the line core argument ($m_L = 0.208/\theta^{0.5}$) is extended to k_s, then a substantial share, ($\alpha_i = \alpha_x - \alpha_L$)

$$\alpha_i \simeq 0.103\ e^2\theta^{12.5} \quad \text{dB/km} \tag{12}$$

is not supported by the H_2O monomer line spectrum ($\theta^{12.5} \simeq 4.3\%/K$).

At this point one might speculate about $(H_2O)_2$ dimer absorption. An estimate of the partial dimer vapor pressure

$$e_D \simeq 3.12 \times 10^{-4}\ e^2\theta^5 \quad \text{kPa}, \tag{13}$$

was obtained by fitting data on physical dimer properties given in Table IV. A strong 138 GHz attenuation rate,

$$\alpha_i \simeq 330\ e_D\theta^{7.5} \quad \text{dB/km}, \tag{14}$$

results when (12) and (13) are combined ($\theta^{7.5} \simeq 2.5\%K$).

TABLE III.

Summary Data of H_2O Line Spectrum and H_2O Excess Attenuation at 137.9 GHz, T=300 K.

a) Experiment-versus-MPM Predictions

	MOIST AIR						DRY AIR	
	k_s	x_s	k_f	x_f	m	x_m	k_d	x_d
	$x10^{-2}$		$x10^{-2}$		$x10^{-2}$		$x10^{-6}$	
X	13.2	10.5	0.570	3.0	4.32	-7.5	2.2	-
M	13.15	10.51	0.5666	3.09	4.309	-7.42	2.10	2.35

b) Local H_2O Lines in MPM (31% of c):

M	0.802	3.5	0.175	3.8	21.8	0.3

c) Complete H_2O Line Spectrum (m = 0.022 assumed - see Table II)

	2.59	3.5	0.57	3.0	22	-0.5

d) Excess H_2O Absorption:

Eq. (12)	10.3	12.5

TABLE IV.

Reported Data on $(H_2O)_2$ Dimer Concentration e_D/e Over the Temperature Range from 300 to 386 K.

T , kPa	300	358.4	367.1	375.9	386.4
e , kPa	2.80	58.27	81.47	111.9	159.3
e_D , kPa	0.0024	0.44	0.76	1.28	2.27
e_D/e , $x10^{-3}$	0.9	7.6	9.4	11.4	14.2
e_D/e^2 , $x10^{-4}$	3.1	1.30	1.15	1.02	0.895
*Reference	[19]	[20]			

3.4 MPM Predictions

Features of the user-friendly atmospheric propagation model MPM-N have been discussed in Section 3.1 The desk computer version is written in IBM Professional FORTRAN with extensive comments that guide the user to appropriate references for specific formulations. Three parametric presentations have been found useful in practical applications, which are addressed in separate subprograms:

Profiles	Variable	Parameters
A. Frequency	f	-, P, T, RH(v), w_A, w, R
B. Humidity	RH,v	f, P, T, - , w_A, w
C. Pressure	P	f, -, T, RH(e)

A copy of the opening lines of program MPM-N/A (frequency profiles) is shown in Figure 6. The detailed structure of MPM comes best to light in graphical examples. Typical sea level behavior of MPM-predicted rates, α and β, is illustrated in Figures 7 to 13. Across the millimeter-wave spectrum (Figures 7 and 8) one recognizes more or less transparent window ranges (W1 to W5, separated by molecular resonance peaks. Calculations of total radio path attenuation A[dB], delay B[ps], and atmospheric noise temperature T_A[K] require distributions of P(x), T(x) along the propagation direction x to be known [6].

Spectroscopic properties of the air-broadened water vapor line centered at 183 GHz are demonstrated in Figure 9. Accuracy of supporting line parameters (stength, width, shift) determines the reliability of predictions needed for remote sensing applications with respect to atmospheric humidity. With respect to line shape studies one observes that wing data from the delay spectrum $\beta(f)$ are unaffected by dry air pressure p. Outside a line-center frequency range $\nu_o \pm 5\gamma$, dispersion N'(f) is independent of a particular shape function F'(f) such as (9b)-A.

```
C       PROGRAM MPM-N
C       JULY 1987
C-----------------------------------------------------------------------
C       COMPLEX RADIO REFRACTIVITY OF ATMOSPHERIC AIR (1 TO 1000 GHz).
C       Hans J. Liebe
C       Institute for Telecommunication Sciences
C       NTIA/ITS.S3
C       325 BROADWAY
C       Boulder, CO  80303
C
C       Adapted for IBM-PC Professional FORTRAN  by:
C               John Stricklen   (1-303-497-3195, FTS 320-3195)
C
C       Contents:
C       A. FREQUENCY PROFILES
C       C. PRESSURES PROFILES OF MOIST AIR
C       B. HUMIDITY  PROFILES
C-----------------------------------------------------------------------
C                     A. FREQUENCY PROFILES
C-----------------------------------------------------------------------
C  Program MPM-N/A calculates frequency profiles of the complex radio
C  refractivity N of ATMOSPHERIC AIR over a frequency range f=1 to
C  1000 GHz. The output is expressed in Real part of N and
C  Imaginary part of N and specific rates of power attenuation A
C  (Im. of N) and propagation delay B (Re. of N).
C
C                         OUTPUT:
C         *  Real part of refractivity        N' (f)  in   ppm
C         *  Imaginary part of refractivity   N''(f)  in   ppm
C         *  Nondispersive Refractivity       No      in   ppm
C  or
C         *  Attenuation                      A(f)    in   dB/km
C         *  Dispersive Delay                 B(f)    in   ps/km
C         *  Refractive Delay                 Bo      in   ps/km
C
C
C  Frequency range, moist air, rain conditions (specified by five
C  meterological variables P=p+e, T, RH, wA or w, RR), and haze model
C  code (A, B, C, or D) are the required input information to be
C  entered from the keyboard.
C
C                         INPUT:                          Valid Range:
C         *  Frequency range      f1, f2     in GHz       1 to 1000
C              and step size          df     in GHz       >= 1.E-05
C                                                         (max. 500 freqs.)
C         *  Barometric pressure     P       in kPa       0.0  to 120
C         *  Temperature             T       in  C        -50 to 50
C         *  Relative humidity       RH      in  %        0 to 100
C             [absolute humidity is calculated as v(RH,T) in g/m3
C                                              or e(RH,T) in kPa.]
C         *  Haze model (RH = 80 to 99.9%):
C             code A(rural), B(urban), C(maritime), and D(C +strong wind)
C             plus hygroscopic aerosol reference
C             concentration      wA(80%RH) in mg/m3     0 to 1
C         *  Suspended water droplet
C             concentration          w       in g/m3      0 to 10
C         *  Rain Rate              RR      in mm/hr     0 to 200
C
C  COMMENTS:
C  The computation of attenuation A and delay B is described in
C  References [1] to [3].
C
C  MOLECULAR effects due to oxygen, nitrogen, and water vapor
```

Figure 6. Opening lines (total = 1350) of MPM-N/A PC-computer program listing.

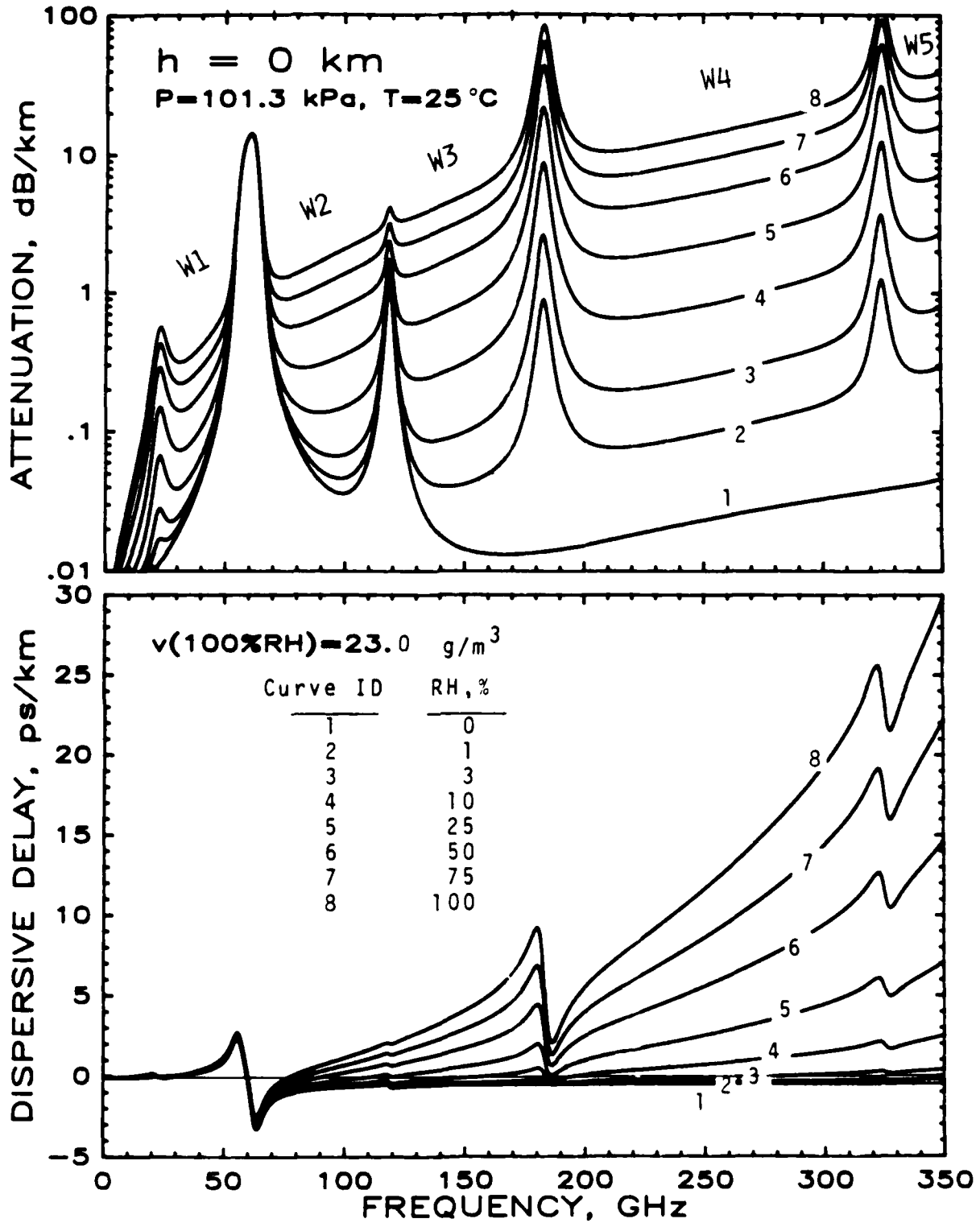

Figure 7. MPM-predicted specific values of attenuation α and dispersive delay β at sea level height h=0 km (P=101.3 kPa, T=25°C, RH=0 to 100%) over the frequency range, f=1 to 350 GHz. Window ranges are marked W1 to W5.

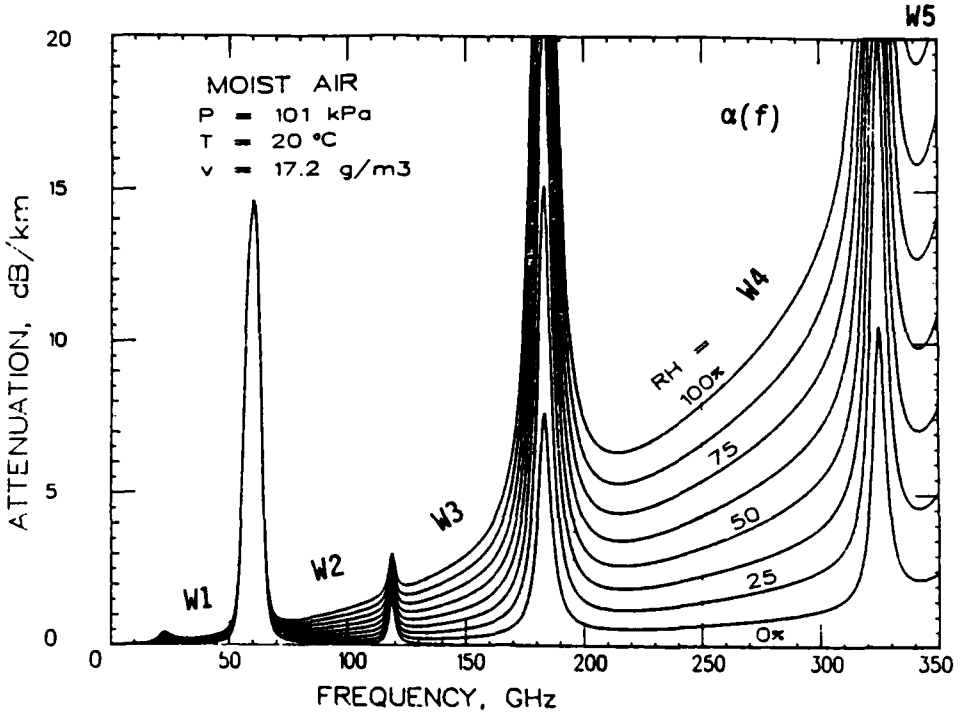

Figure 8. Water vapor absorption in window ranges for constant relative humidity increments (ΔRH = 12.5%) at a sea level condition.

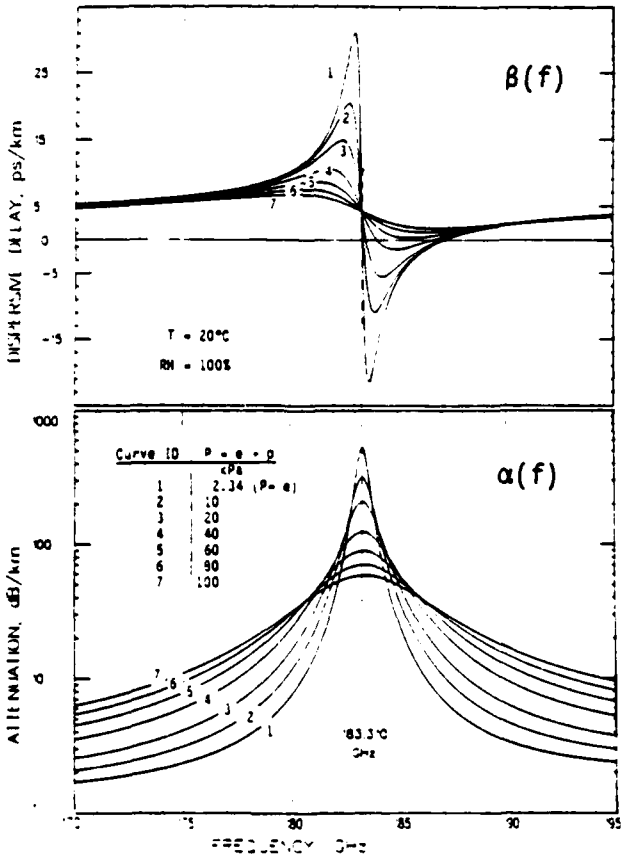

Figure 9. Pressure-broadening (AIR) example of the 183 GHz H_2O line.

A major concern for most NMMW systems is their performance in rain. A simplified classification of rain events is given in Section 1.1 of the Appendix. When neglecting any statistical nature of rain within a radio path, the calculation scheme (18)-A provides a rough estimate on $\alpha(f)$ and $\beta(f)$. Predictions (Figure 10) are based on adding to the known state of moist air (P-T-RH) only one additional parameter, namely the point rain fall rate R.

Of some importance is the fog/cloud prediction program in MPM. Systems operating in the NMMW range offer an attractive alternative to electro-optical systems when operation has to be assured during periods of adverse weather (rain, cloud, fog, haze, high humidity). Current interest is focused on the frequency range 90 to 350 GHz where an optimum trade-off between atmospheric obscurations and angular resolution can be achieved [11]. All atmospheric loss and delay effects have to be known accurately in order to analyze the potential for all-weather performance. The suspended water droplet (SWD) formulation (16)-A, (17)-A of MPM is an addition to the state of saturated air (P-T-RH=100%) as illustrated in Figure 11. Key parameters are SWD content w in g/m^3 and temperature T in °C.

Another atmospheric ingredient is the mass concentration w_A of hygroscopic aerosol (HAE). Solution droplets appear for RH > 80%, and haze conditions develop as RH approaches 100 percent. These conditions can be modeled by assuming that at the reference humidity, RH = 80%, the HAE concentration $w_A(RH = 80\%)$ is known. The RH dependent swelling/shrinking w(RH) is described approximately up to RH = 99.9% by a growth model (3)-A.

Relative humidity RH is the variable that governs physical processes taking place in the atmosphere with respect to water vapor. Practical models for RH parameterization exceeding saturation are not available. Both, absolute humidity (v), and suspended haze droplet concentration (w_A), however, can be expressed in terms of RH variability. Absolute (v) and relative (RH) humidity are interrelated through the ambient temperature T.

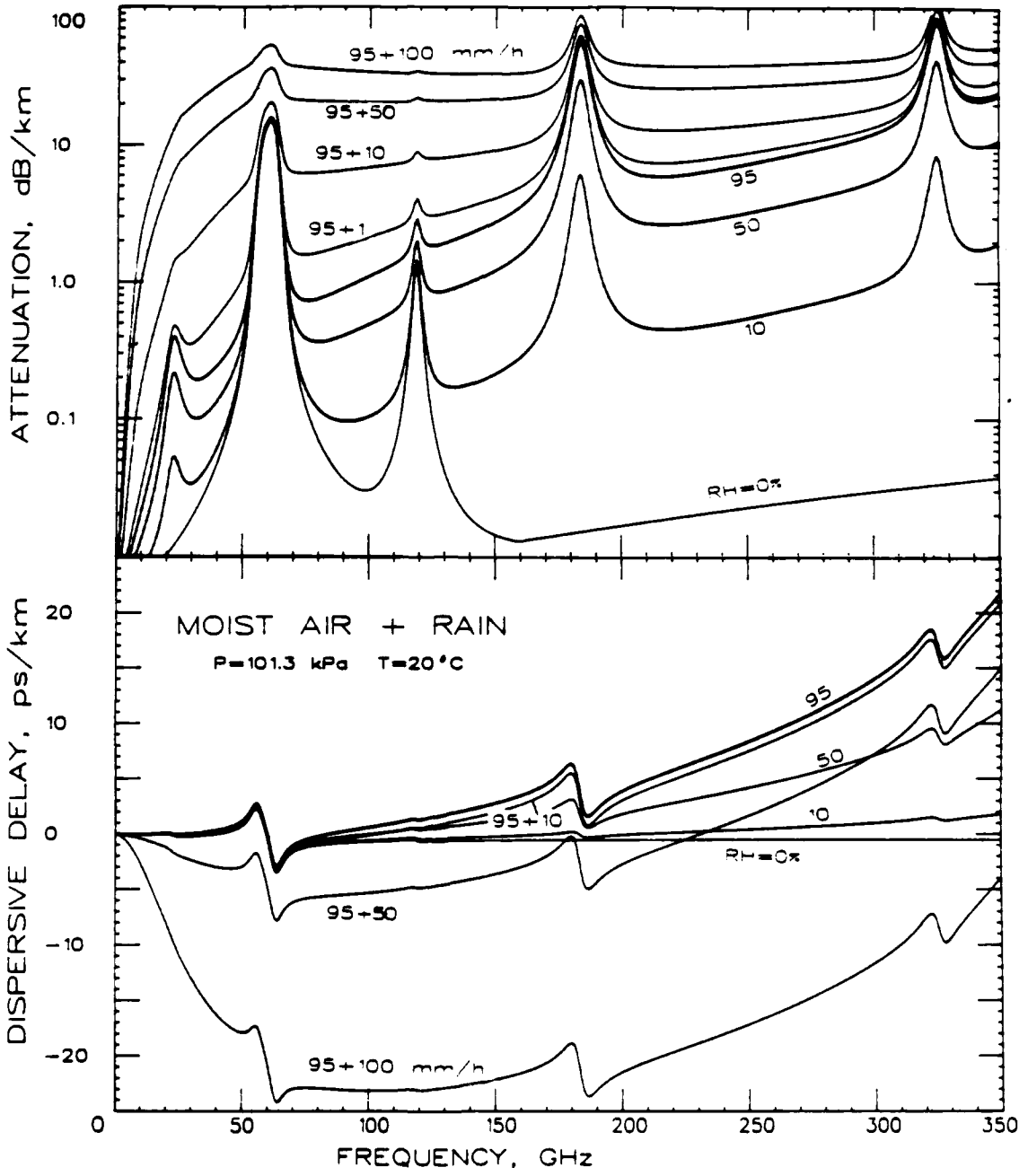

Figure 10. Attenuation α and delay β rates for three rain events (R=10, 50, and 100 mm/h) added to a moist air (RH=90%) sea level condition. Also shown are dry air (0% RH) and moist air (50% RH) characteristics.

Sulfates are the major RH-active ingredient of both urban and rural aerosols; so is sodium chloride for maritime species. The atmosphere is never free from HAE, with greatest concentrations near the surface and scale heights on the order of 1 km. Above RH = 90%, suspended water droplets have developed carrying the HAE essence in solutions. Average values of w_A lie between 0.01 and 1 mg/m^3. The humidity parameterization in MPM is demonstrated by the examples given in Figures 12 and 13.

Pressure variability comes into play when modeling height dependencies. Cumulative calculations of α/β for a slanted radio path through the neutral atmosphere (e.g., ground-to-satellite) encounter pressures, P = 100 to 0 kPa, which narrows the molecular absorption lines until they vanish altogether. Pressure-, Zeeman-, and Doppler-broadening [(11)-A] have to be considered over the height range:0 to 90 km. Another need for a formulation of pressure profiles arises from spectroscopic studies applying pressure-scanning techniques. A simulation of laboratory measurements discussed in Section 2.3 is exhibited in Figure 14.

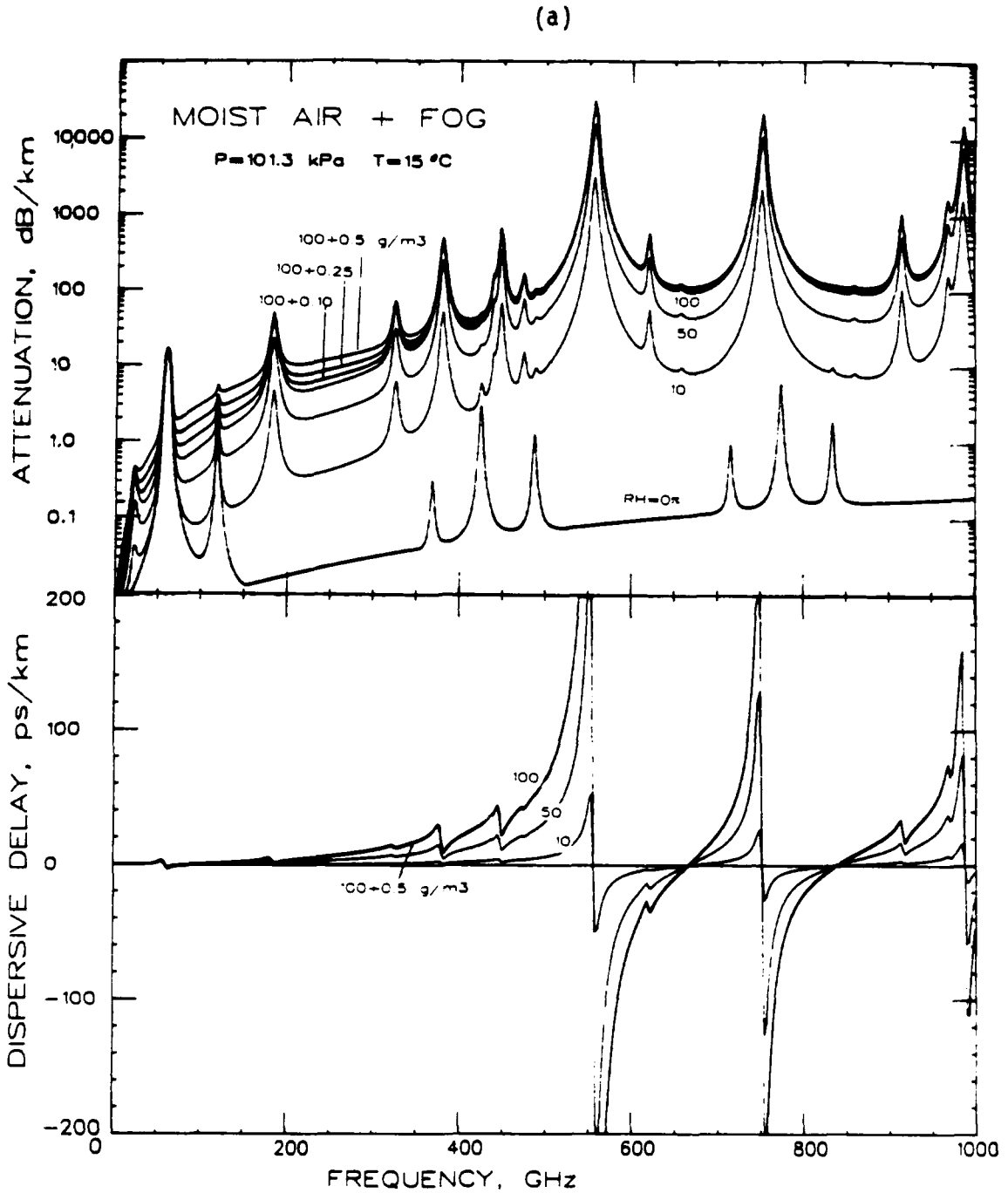

Figure 11. Attenuation α and delay β rates for three fog events (w = 0.10, 0.25, and 0.5 g/m^3) added to a saturated air (RH=100%) sea level condition. Also shown are dry air (0% RH) and moist air (50% RH) characteristics: (a) f = 1-1000 GHz,

(b)

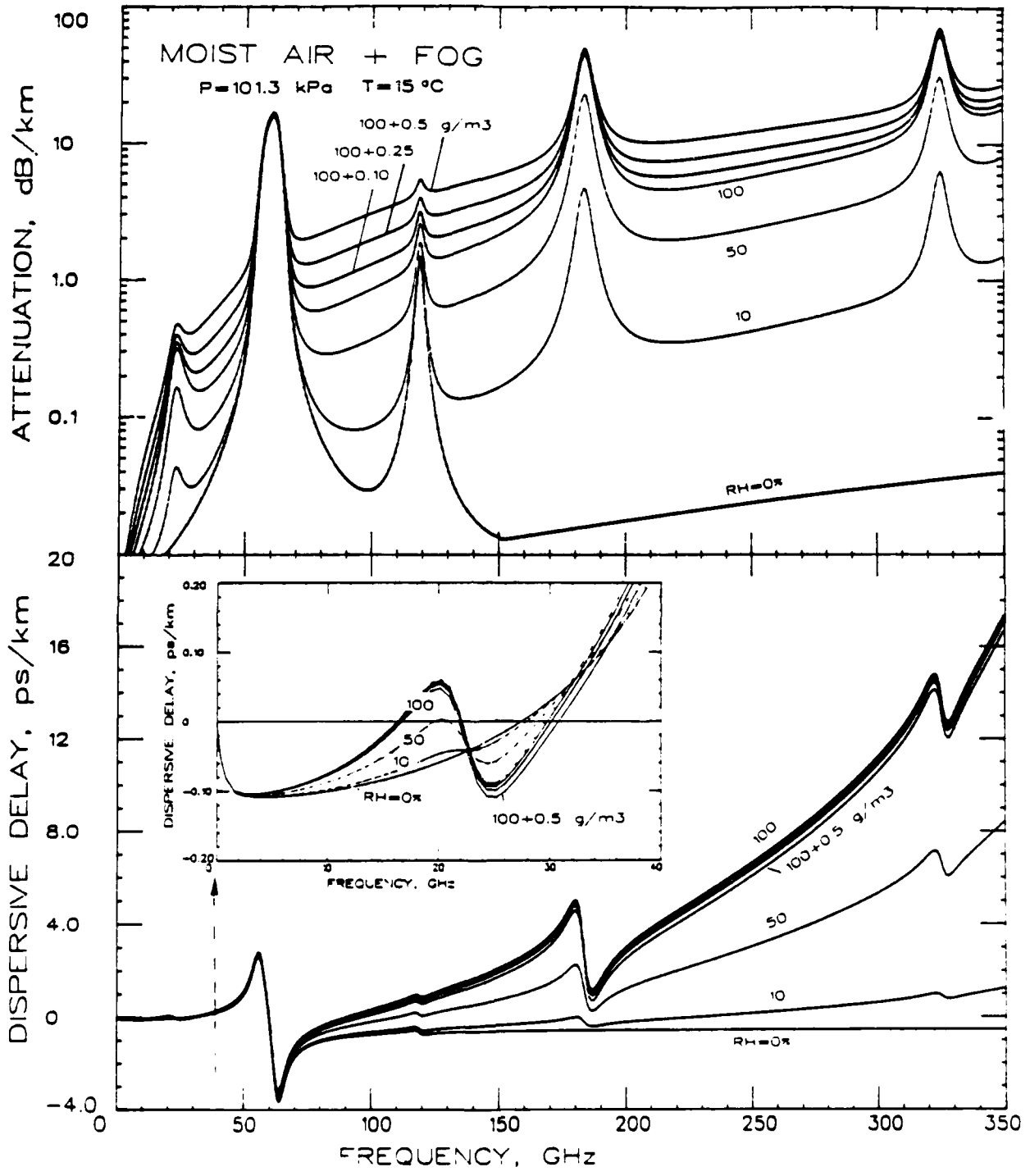

Figure 11. continued: (b) f = 1-350 GHz and f = 0-40 GHz (insert).

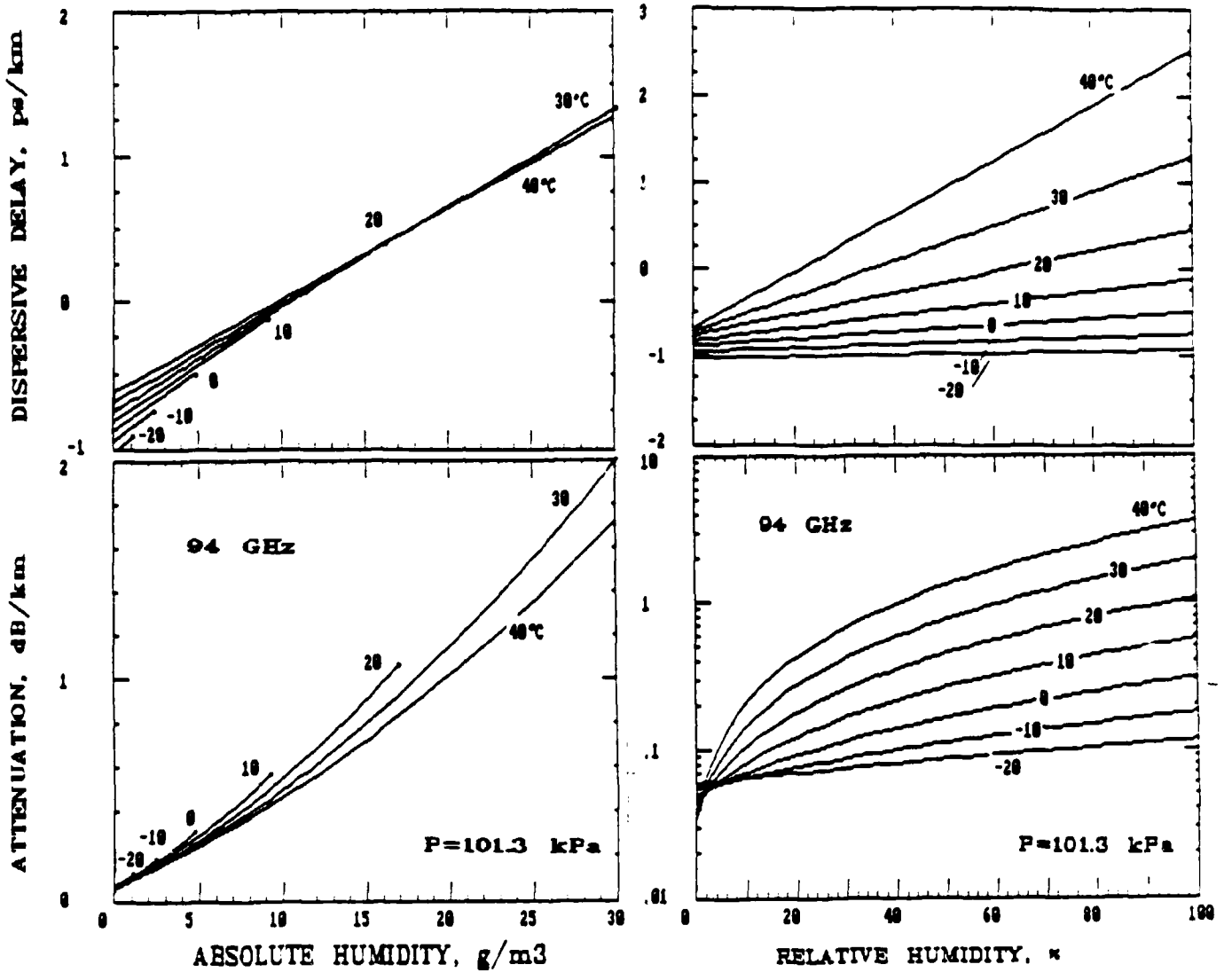

Figure 12. Absolute (v) and relative (RH) humidity dependence of attenuation α and delay β at f = 94 GHz for various sea level conditions (P = 101.3 kPa and T = -20 to 40°C).

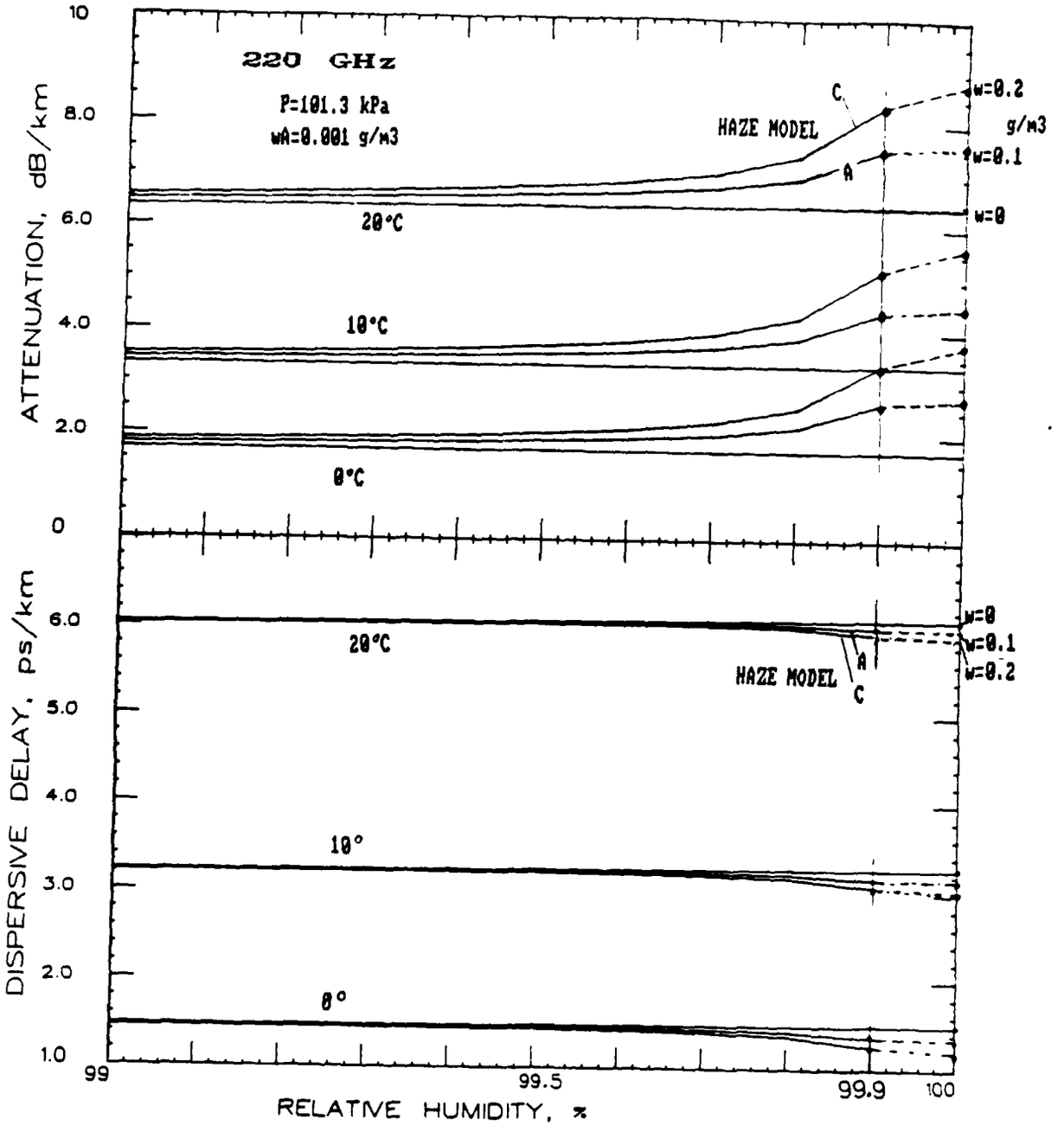

Figure 13. Two haze cases (A:1 mg/m^3 and C:1 mg/m^3) for prefog (RH = 99-99.9%) and fog (w=0.1 and 0.2 g/m^3) conditions at three temperatures (0, 10, 20°C) displaying the associated attenuation α and delay β rates at f = 220 GHz.

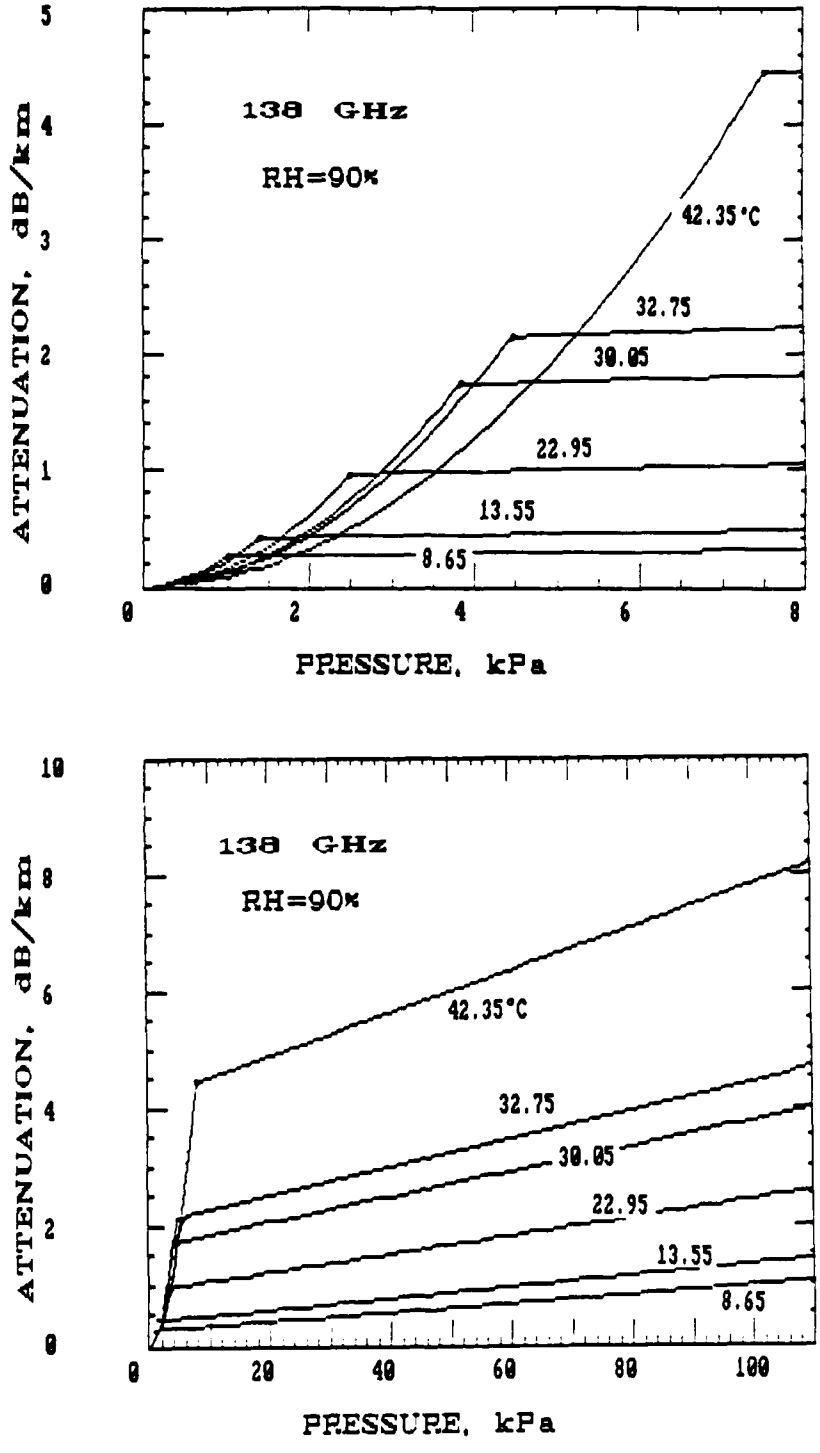

Figure 14. Pressure profiles at f = 138 GHz simulating the laboratory attenuation measurements presented in Section 2.3.

4. EXPERIMENTAL-VERSUS-MODEL (MPM) DATA

Corroborative experimental data of sufficient quality to scrutinize MPM predictions are scarce. Reliability, precision, and limited scope of supporting meteorological data often compromise the accuracy of results deduced from field observations. Generally, laboratory experiments are more accurate by simulating controlled electromagnetic and atmospheric conditions crucial to validate a specific model aspect. In this manner, contributions from the 22 and 183 GHz water vapor lines and from the 48 to 70, 119 GHz oxygen lines have been evaluated [3], [13], [15], [16], [23]. In many cases, theoretical refinements are motivated to improve the interpretation of empirical laboratory data by establishing a connection to the physics of the problem. For example, a set of our unpublished dispersion (N') results on dry air, taken during 1976 between 53.6 and 63.6 GHz, provided reference data for an elaborate reformulation of interference coefficients that describe the 60 GHz O_2 bandshape [23]. The new coefficients were adapted for MPM, and Table V elucidates the degree of agreement.

4.1 Laboratory Measurements

The results on moist air attenuation at 138 GHz [i.e., (5), (8)] provided clues to a formulation of an empirical MPM water vapor continuum. Data from other workers were evaluated to check if the assumptions of (10) held up at different frequencies. Water vapor attenuation at frequencies between 330 and 430 GHz is compared with MPM predictions in Figure 15. The data were available in graphic form and had to be digitized by us. Considering the many difficulties that plague absolute calibrations, a comparison of model-vs.-experiment is encouraging. No anomalous absorption features have been uncovered.

Two laboratory studies of the 183 GHz water vapor line have been reported by a French group [15], [16]. We adapted the width results [15] for the line table of MPM. A detailed analysis of temperature-dependent wing data [16] is given in Table VI. Equation (5) was applied to reduce both, experimental and MPM data, for a mutual comparison. At +1 GHz from the line center, the attenuation rate for pure water-vapor displays a 21 percent discrepancy. The origin of such disagreement has to be attributed to 183 GHz line broadening problems but not to the rather small contribution from the continuum.

TABLE V.

Measured (EXP) and Predicted (MPM) Dispersion in Dry Air at 300 K (MPM uses interference coefficients from Rosenkranz [23]).

Nearby Line	Frequency	Dispersion N'(f) EXP | MPM p = 53.3 kPa		Frequency	Dispersion N'(f) EXP | MPM p = 80.0 kPa	
	GHz	ppm		GHz	ppm	
25-	53.588	0.30	0.300	53.584	0.43	0.438
23-	54.123	0.35	0.339	54.119	0.50	0.489
19-	55.214	0.40	0.408	55.210	0.58	0.576
17-	55.776	0.42	0.423	55.772	0.60	0.591
15-	56.356	0.41	0.399	56.352	0.59	0.564
13-	56.960	0.38	0.348	56.956	0.45	0.498
3+	58.439	0.19	0.174	58.435	0.26	0.249
7-	59.156	0.08	0.075	59.152	0.12	0.108
5+	59.583	0.03	0.027	59.579	0.03	0.030
5-	60.296	-0.075	-0.084	60.292	-0.11	-0.132
7+	60.425	-0.135	-0.123	60.421	-0.17	-0.171
9+	61.140	-0.275	-0.252	61.136	-0.383	-0.357
11+	61.790	-0.335	-0.336	61.786	-0.510	-0.516
13+	62.400	-0.480	-0.474	62.396	-0.685	-0.680
3-	62.475	-0.510	-0.495	62.471	-0.720	-0.701
15+	62.297	-0.590	-0.579	62.983	-0.80	-0.797
17+	63.558	-0.610	-0.591	63.554	-0.841	-0.842

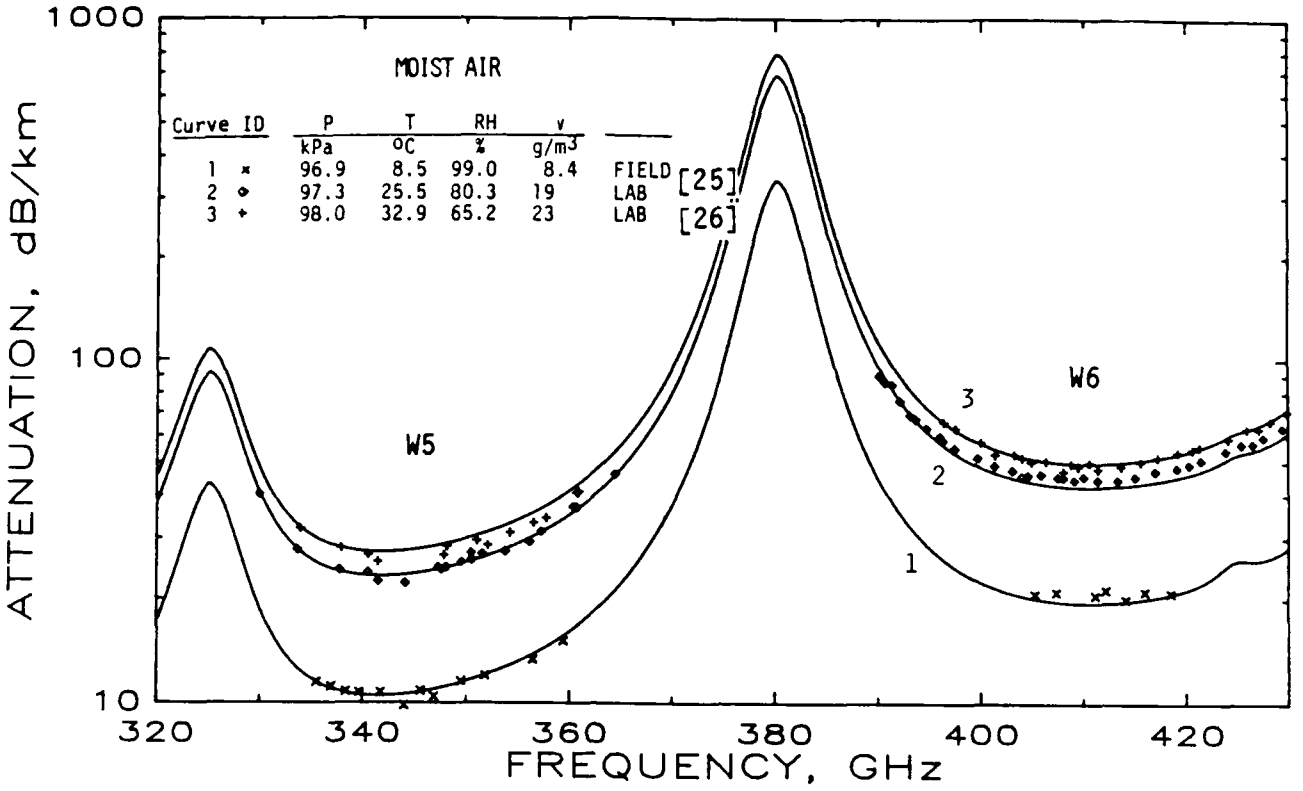

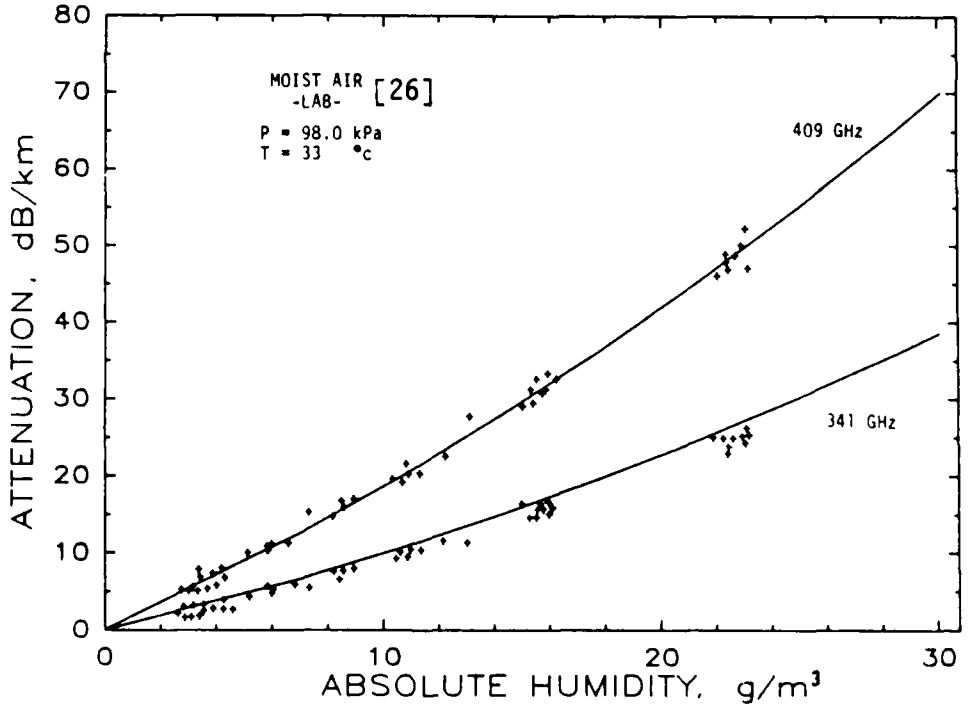

Figure 15. Moist air attenuation rates α across the atmospheric window ranges W5 and W6 (320 to 430 GHz) at temperature 8.5, 25.5, and 32.9°C: measured data [25], [26]; solid lines, MPM.

TABLE VI.

Comparison Between MPM-Predicted and Experimental Attenuation for Water Vapor (e) and Moist Air ($P = e_1 + p$) in the Wing Region of the H_2O Line Centered at ν_o = 183.310 GHz.

f, GHz		ν_o + 3.0			ν_o + 1.0			ν_o + 0.4		
MPM - PREDICTIONS										
	e_1	1.766kPa (13.25 torr)			1.059kPa (7.94 torr)			0.529kPa (3.97 torr)		
	T/K	Lines	Cont.	Total	Lines	Cont.	Total	Lines	Cont.	Total
α, dB/km	310	3.66	0.53	4.19	11.35	0.19	11.54	17.37	0.05	17.41
	300	4.17	0.70	4.87	12.90	0.25	13.15	19.73	0.06	19.79
	290	4.76	0.95	5.71	14.17	0.33	15.05	22.49	0.08	22.58
	P	100kPa (750 torr)			100kPa (750 torr)			100kPa (750 torr)		
α, dB/km	310	21.52	1.83	23.52	21.39	0.95	22.52	11.66	0.43	12.27
	300	23.59	2.07	25.86	23.10	1.06	24.35	12.57	0.47	13.24
	290	25.92	2.40	28.53	25.00	1.19	26.41	13.58	0.51	14.31
DATA REDUCTION: MPM-vs-EXPERIMENT										
		MPM	EXP*	X/M %	MPM	EXP*	X/M %	MPM	EXP*	X/M %
k_s	300	1.56	1.67	7.1	11.72	14.2	21.2	70.56	75.3	6.7
x_s	-	4.56	4.1	-10.1	3.99	3.9	-2.3	3.88	3.5	-9.8
k_f	300	0.121	0.136†	12.4	0.107	-			N.A.	
x_f	-	2.48	2.7	8.9	1.96	-			N.A.	
m	300	0.0776	0.0814	4.9	0.0913	-			N.A.	

*Reference [16],

†N_2-result reduced by 0.907.

4.2 Field Measurements

Ultimately, it is up to field experiments to garner realistic evidence in support of model predictions. When conducted with care at different locations under a variety of natural conditions, such experiments prove to be quite costly.

Data from ITS field studies on the propagation of millimeter waves were evaluated for water-vapor attenuation rates at 96.1 GHz. Comparison between clear air data and MPM predictions shows close agreement, including for the temperature dependence, as demonstrated in Figure 16. The mission of these experiments was to establish a data base for 11.4 to 96.1 GHz propagation in a humid climate (Huntsville, AL: April - August 1986). A similar comparison was not so favorable for a set of data displayed in Figure 17. The results were obtained over a 1.5 km line-of-sight path in the Soviet Union at sub-freezing temperatures for frequencies between 192 and 260 GHz [24]. Experimental uncertainties are not discussed, the extreme environmental conditions may have played a role. On the other hand, 335 - 420 GHz field data (included in Figure 15), that were reported by another group from the Soviet Union [25], agree remarkably well with MPM predictions.

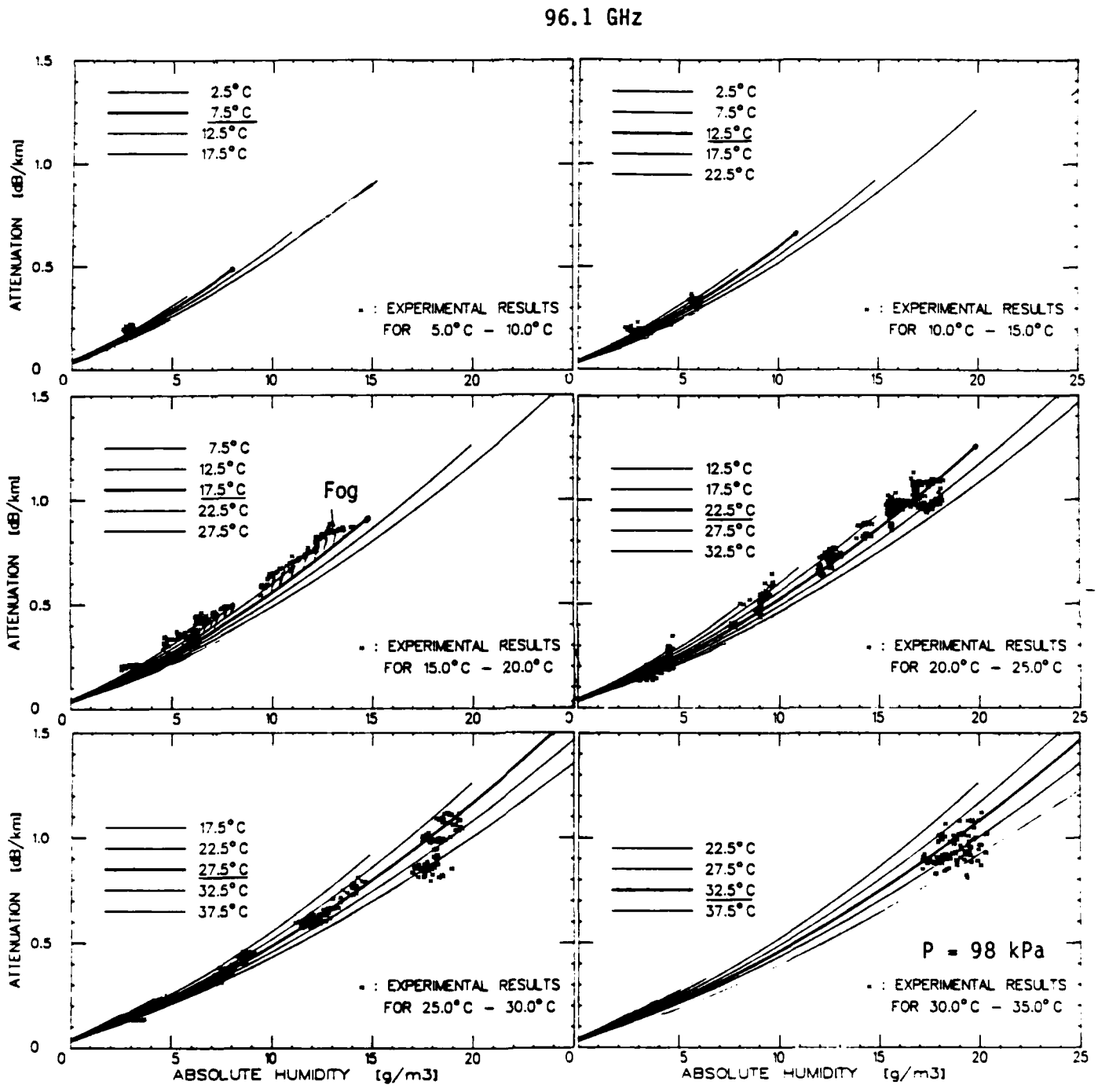

Figure 16. Moist air attenuation $\alpha(v)$ measured at 96.1 GHz over a 21.4 km line-of-sight path located in Huntsville, AL ($h \simeq 0.3$ km) for 6 temperature groups between 2.5 and 37.5°C [Manabe et al., private communication, 1987]: x= 5 min averages for 4.5 days (5/4-6, 8/15-16/1986); solid lines, MPM.

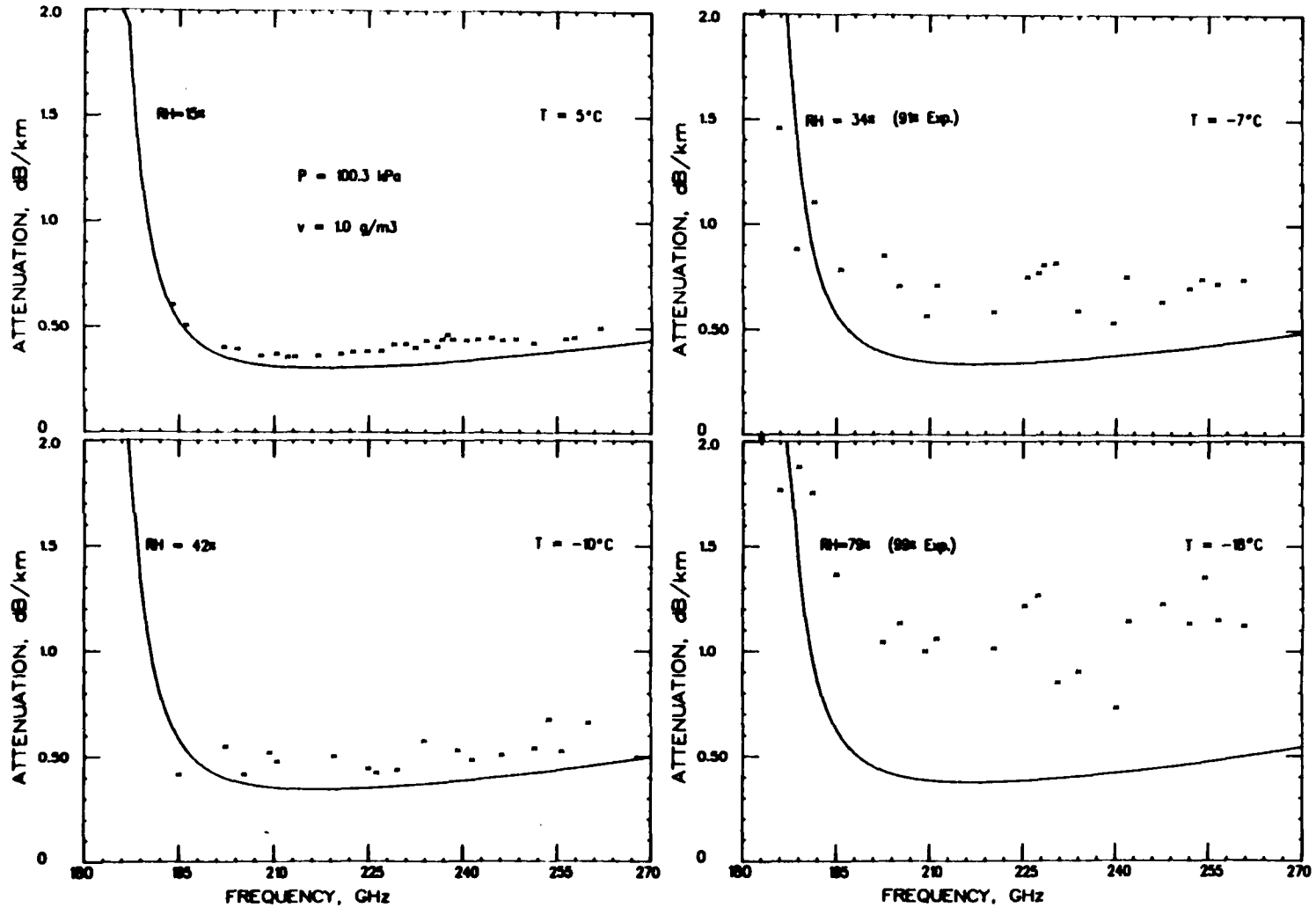

Figure 17. Water vapor attenuation rates α(v) across the atmospheric window range W4 at four temperatures, 5, -7, -10, and -18°C: data points [24]; solid lines, MPM.

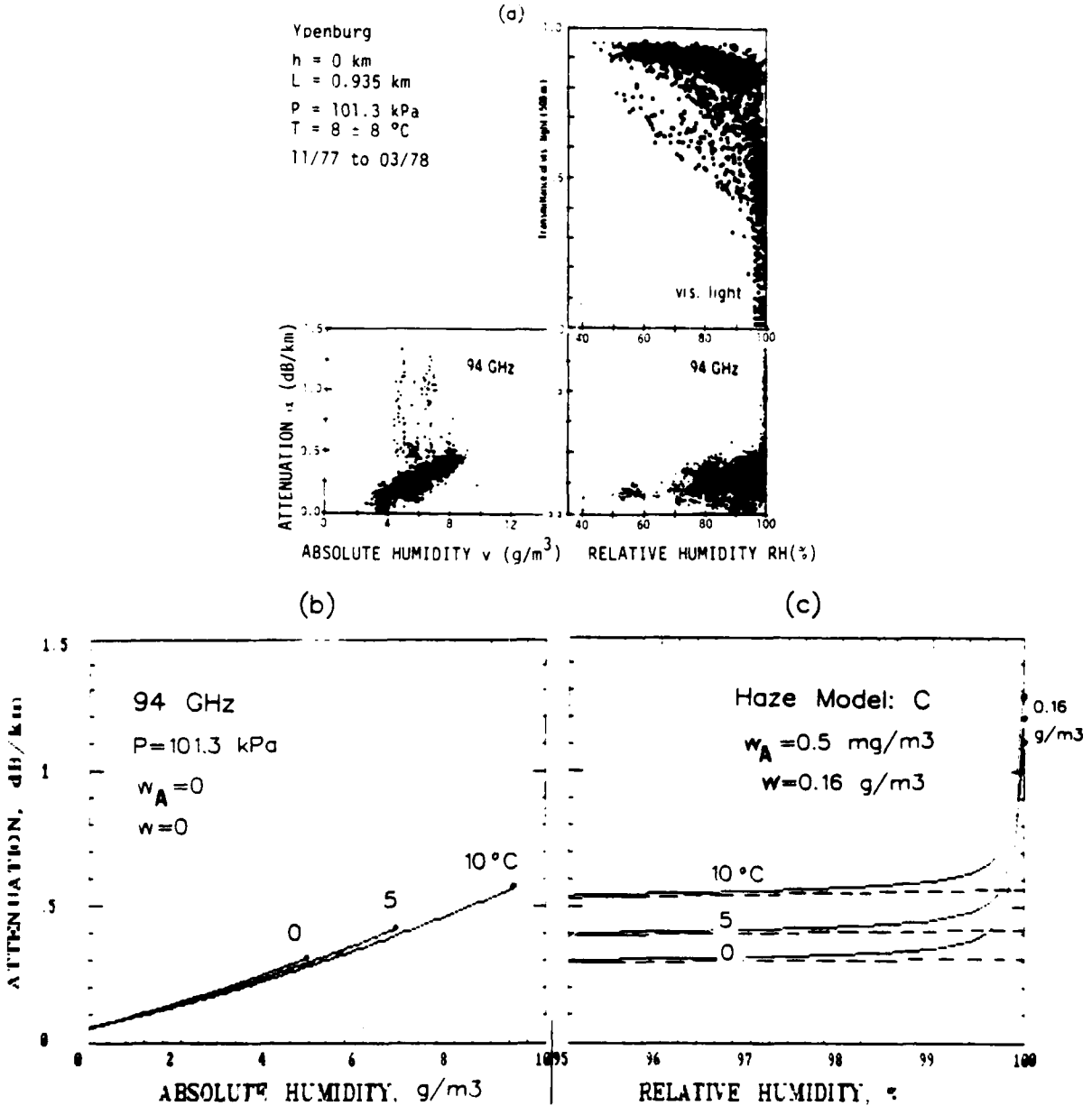

Figure 18. Terrestrial path attenuation at 94 GHz and 0.65 μm (visible light) under nonprecipitating conditions as a function of absolute (v) and relative (RH) humidity [8]: (a) data points, 5 min averages taken every 30 min during a period of 4 months; (b) MPM simulation of (a) for absolute humidity; (c) MPM simulation of (a) over the range, RH=95 to 100%, including haze model C.

Attenuation data at 94 GHz have been recorded in a coastal region of the Netherlands [8]. Data, when presented in Figure 18 versus absolute humidity v display significant random excess attenuation over MPM predictions. The same data plotted versus RH places all excess attenuation at RH > 98%. Haze and fog conditions probably were present as evident from optical transmission data. The highest excess of 0.8 dB/km requires w 0.16 g/m^3 which is typical for heavy fog.

Figure 19 presents atmospheric noise temperatures measured against zenith at two different sites simultaneously at 10, 33, and 90 GHz [27]. Predictions with the MPM radio path program reproduce the frequency correlations quite correctly which tends to confirm the f^2 assumption made for H_2O continuum absorption (10). In addition, model data set a limit for total precipitable water vapor V[mm] carried by the air mass. Noise exceeding this limit probably originates from suspended droplets. Data trends stemming from differences in the f-dependence of moist air and SWD absorption support such assumption.

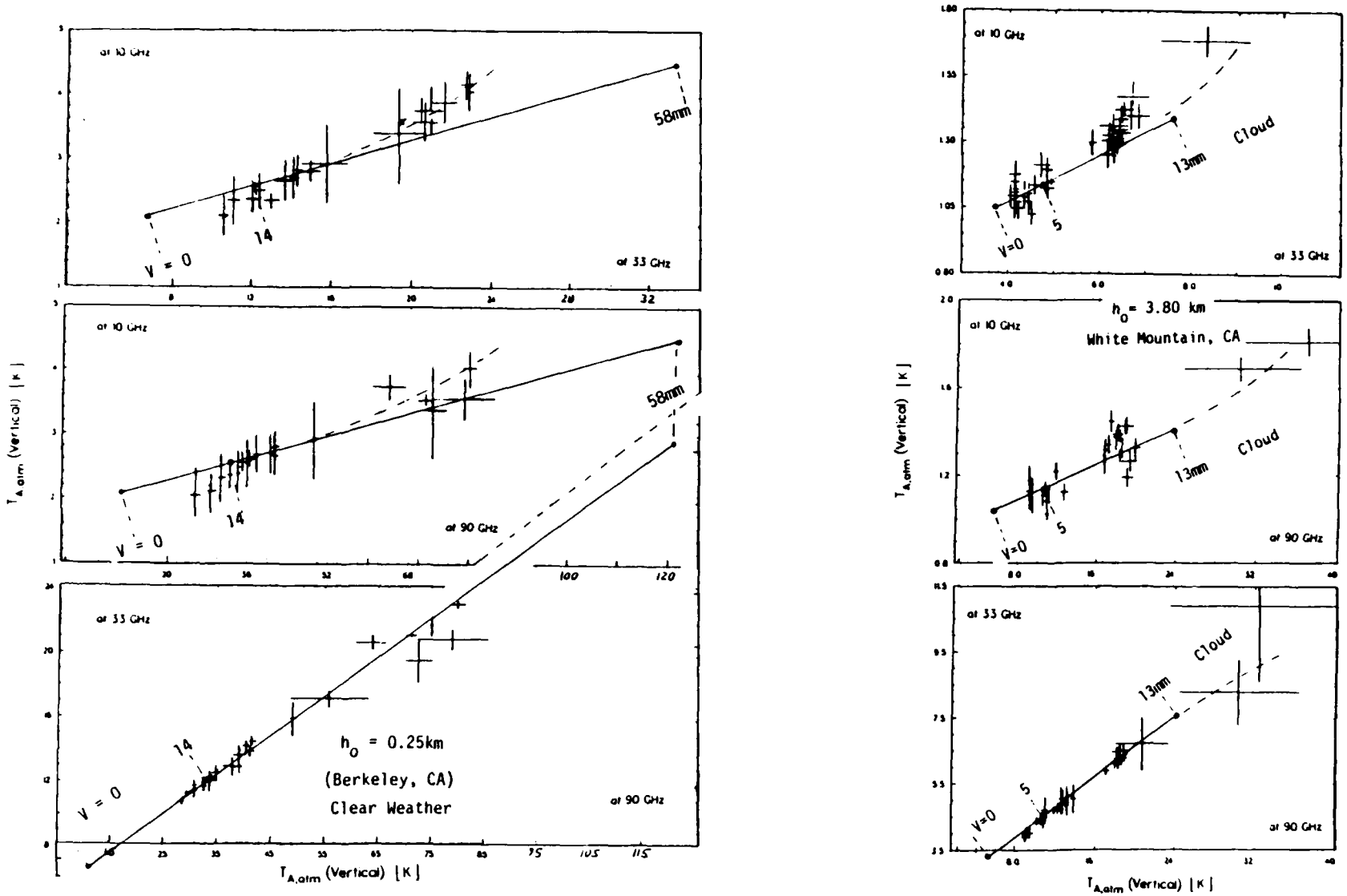

Figure 19. Correlated vertical atmospheric noise temperatures T_A at the frequency pairs 10/33, 10/90, and 33/90 GHz. Path-integrated water vapor is $V = \int v dh$, mm. The measurements were conducted from two sites located at height levels h_0=0.25 and 3.30 km: data points [27]; solid lines, MPM with a mean July height profile (0-30 km) of P, T, RH for San Francisco, CA [8].

5. CONCLUSIONS

Radio properties of the atmosphere are both a barrier and a boon to application programs in the 100 - 1000 GHz (NMMW) spectral range. The first part of this report gave a somewhat detailed description of a laboratory experiment that had to apply latest advances in digital electronics and cryogenic detection for the sole purpose of coming up with no more than two attenuation coefficients, k_s and k_f (8) at 138 GHz. At first sight, these two quantities describe the attenuation rate of moist air over a rather inconspicuous range from 0.1 to 10 dB/km; however, a more detailed analysis revealed: the k-formulation provides conclusive evidence on temperature and pressure dependences of the water vapor continuum. Attaching an f^2 dependence to the 138 GHz results turned a frequency-limited (< 1 THz), propagation model into a useful tool capable of operating in frequency, humidity, and pressure domains of the atmosphere (see Section 3.1).

The report discussed details of contributions to modeling atmospheric NMMW properties, foremost the attenuation calibration of MPM employing new laboratory results on moist air. Water vapor continuum absorption and, above RH = 90%, droplet attenuation are both affected by relative humidity RH. For haze formation, the range up to RH = 99.9% was modeled. So far, in fog and cloud situations, when RH exceeds 100 percent, values for w cannot be model-generated from the atmospheric water vapor pool.

The code MPM was readily accepted by radio scientists and engineers. About 90 requests for copies of MPM have been honored since January 1986. Quotes from received comment were encouraging: "MPM proved of considerable value," - "documentation is about the best I have ever seen," - "technical flow, model development and general visibility for application efforts is superior," etc. The Microwave Group of the International Radiation Commission largely adapted MPM as atmospheric transmission code (i.e., 30 times referenced in "Report of Microwave Group on ITRA," March 1987).

Although MPM was found capable of predicting atmospheric NMMW propagation limitations, several shortcomings still exist. They are, for example, the missing confirmation for a physical basis of water vapor continuum absorption (e.g., [17], [18]) dominating transmission in atmospheric window ranges centered at 90, 140, 220, 340 GHz and higher; needed measurements of spectroscopic parameters (i.e., shape, strength, width and shift) for spectral lines of the main absorbers (O_2 and H_2O) over the full atmospheric temperature range (300-200 K); and a lack for reliable subfreezing transmission data to clarify the problems that are indicated by Figure 17. Further parametric (frequency, pressure, humidity, temperature, gas composition such as H_2O + AIR) studies are proposed to realize the benefits obtainable from the high-humidity performance of the spectrometer that has been perfected overcoming a great deal of difficulties. Pressure-broadening of the 183 GHz line uniquely identifies monomer behavior (see Table VI). A comparative study of wing (f_o ±6 GHz) and far-wing (220 GHz) responses to T and v(RH) variations would allow an apportioning of local line (known) and continuum (unknown) contributions.

6. LIST OF PUBLICATIONS*

A. Manuscripts Published Under ARO Sponsorship

(25 copies each have been forwarded to ARO Information Processing)

[1] Liebe, H., V. Wolfe, and D. Howe,
"Test of wall coatings for controlled moist air experiments",
Rev. Sci. Instr. 55 (10), 1702-1705, October 1984.
[ARO 101-83]

[2] Liebe, H., K. Allen, G. Hand, R. Espeland, and E. Violette,
"Millimeter-Wave Propagation in Moist Air: Model Versus Path Data"
NTIA Report 85-171, March 1985, 62 pp. (NTIS Order No. PB 85-208700).
[ARO 111-85]

[3] Liebe, H. J.,
"An updated model for millimeter wave propagation in moist air",
Radio Science 20 (5), 1069-1089, September-October 1985; and
[ARO 111-85]

[3a] ibid,
ARO Report No. 21677.2-GS.

[4] Liebe, H. J. and D. H. Layton,
"Studies of moist air properties up to 1 THz",
Proc. 10th Int'l. Conf. IR & MM Waves, Lake Buena Vista, FL, Dec. 1985
(IEEE Cat. No. 85CH2204-6, M7.3, p. 69-70).
[ARO 111-85]

[5] Liebe, H. J.,
"Modeling millimeter wave propagation in moist air",
Int'l. Conf. Optical and Millimeter Wave Propagation and Scattering in the Atmosphere, Florence, Italy, May 27-30, 1986 (Conference Digest, p. 203-206).
[ARO 107-86]

[6] Hopponen, J. and H. Liebe,
"A computational model for the simulation of millimeter-wave propagation through the clear atmosphere",
NTIA Report 86-204, October 1986, 32 pp. (NTIS Order No. PB 87-131173/AS).
[ARO 107-86]

*AVAILABILITY OF PUBLICATIONS -
Requests for copies of journal articles should be addressed to the journal. NTIA Reports are available via the order number from the National Technical Information Service, 5285 Port Royal Road, Springfield, VA 22161. Technical Memoranda and Internal Reports are not generally available, but additional information may be secured by contacting the author.

[7] Liebe, H. J.,
"Relative-humidity parameterization for atmospheric millimeter wave propagation modeling,"
Proc. Int'l. Open Symposium, URSI-Comm. F, Durham, N.H., 7/28-8/1, 1986; Paper 6-4/1 to 4.
[ARO 107-86]

[8] Liebe, H. J.,
"A contribution to modeling atmospheric millimeter-wave properties",
FREQUENZ (Telecom. J.) 41 (1/2), 31-36, 1987.
[ARO 107-86]

[9] E. Miller, editor (H. Liebe and J. Stricklen),
"PC's for AP: ITS's program MPM-N",
IEEE APS Newsl. 28 (5), 29-30, 1986.

[10] Liebe, H. J. and D. Layton,
"Near-millimeter-wave attenuation and delay rates by moist air",
Proc. Int'l. Geosc. & Remote Sensing Symp.-IGARSS' 87, MP-1-8, p. 13-14; Ann Arbor, MI, May 1987.
[ARO 107-86]

B. Related Reports

(1 copy each has been forwarded to ARO)

[11] Liebe, H. J.,
"Atmospheric mm-wave attenuation", Handout (12-page) at Workshop on Near-MM-Wave Communic. Techn., NY-IT, Dec. 5-7, 1984.
[ARO - sponsored]

[12] Kuenzi, K. F., Editor (S. Clough, N. Grody, K. Kuenzi, H. Liebe, A. Neuendorffer, B. Read, P. Rosenkranz, and C. Warner; Contributors)
"Report of Microwave Group on ITRA-Intercomparison Campaign Workshop,"
University of Maryland, 86 pp., March 1986.

Excerpts (Mm-wave activities) from ITS Annual Progress Reports 1984, 1985, and 1986.

C. Abstracts of Presentations (by H. Liebe)

(1 copy each has been forwarded to ARO)

1. "An updated model for mm-wave propagation in moist air,"
   8th Annual Review Conf. Atm. Trans. Models, AFGL Hanscom AFB, June 4-5, 1985.

2. "Experimental confirmation of the mm-wave propagation code MPM,"
   (with G. Hand and K. Allen), 1985 North American Radio Science Meeting, URSI-F6, Vancouver, June 17-21, 1985.

3. "Features of the mm-wave propagation code MPM,"
   MAS (mm-wave atmosph. sounder) Science Meeting, PENN State University, October 21-22, 1985.

4. "The mm-wave propagation code MPM,"
   ITRA (Intercomp. of Transm. and Radiance Algorithms) Workshop, NASA GSC, October 21-25, 1985 (see [11]).

5. "Millimeter-wave propagation through moist air,"
   EM-Lab Group Meeting, ECE Dept., CU, Boulder, CO, Nov. 1986: Seminar given by J. Stricklen.

6. "Modeling atmospheric refractivity in the near-millimeter-wave range,"
   XXIInd General Assembly of URSI, Tel Aviv, August 1987: Sess. F7.

7. See: [4], [5], [7], [10] - [12].

7. SCIENTIFIC PERSONNEL

	Period
Principal Investigator	
Dr. Hans J. Liebe	10/84 - 3/87
Electronic Engineering	
Donald H. Layton	10/84 - 10/86
Programming	
Kenneth C. Allen	10/84 - 12/84
Gregory R. Hand	10/84 - 1/85
Assistant	
John P. Stricklen, EE graduate student (Prof. E. Kuester, advisor)*	6/85 - 3/87
Guest Scientist	
Dr. Takeshi Manabe†	10/86 - 3/87

8. CONTRACT NUMBERS

ARO Proposal Number: 21677-GS

Contract Number	Period
MIPR ARO 111-85	10/84 - 9/85
MIPR ARO 107-86	10/85 - 3/87

* Dept. of Electrical and Computer Eng., University of Colorado, Boulder, CO 80309.

† Radio Research Laboratory, Tokyo, Japan.

9. REFERENCES

[1]-[12] see 6. LIST OF PUBLICATIONS

[13] Liebe, H. J., and T. A. Dillon, "Accurate foreign-gas-broadening parameters of the 22-GHz H_2O line from refraction spectroscopy," J. Chem. Phys., 50, 727-732, Jan. 1969.

[14] Liebe, H. J., "The atmospheric water vapor continuum below 300 GHz," Int'l. J. Infrared & Millimeter Waves, 5, 207-227, Feb. 1984.

[15] Bauer, A., M., Godon, and B. Duterage, "Self- and air-broadened linewidth of the 183 GHz absorption in water vapor," J. Quant. Spectrosc. Radiat. Transfer, 33, 167-175, Feb. 1985.

[16] Bauer, A., B. Duterage, and M. Godon, "Temperature dependence of water-vapor absorption in the wing of the 183 GHz line," J. Quant. Spectr. Radiat. Transfer, 36, 307-318, Apr. 1986.

[17] Hinderling, J., M. Sigrist, and F. Kneubuehl, "Laser-photoacoustic spectroscopy of water-vapor continuum and line absorption in the 8 to 14 μm atmospheric window," Infrared Phys., 27, 63-120, 1987.

[18] Rosenkranz, P. W., "Pressure broadening of rotational bands. 1. A statistical theory; 2. Water vapor from 300 to 1100 mm^{-1}," J. Chem. Phys., 83, 6139-48, Dec. 1985 (Part 1) and ibid, in press (Part 2).

[19] Suck, S. H., A. E. Wetmore, T. S. Chen, and J. L. Kassner, Jr., "Role of various water clusters in IR absorption in the 8-14-μm window region," Appl. Opt., 21, 1610-1614, May 1982.

[20] Curtiss, L. A., D. J. Frurip, and M. Blander, "Studies of molecular association in H_2O and D_2O vapors by measurements of thermal conductivity," J. Chem. Phys., 71, 2703-2711, Sept. 1979.

[21] Read, W., K. Hillig II, E. Cohen, and H. Pickett, "The measurement of absolute absorption of millimeter radiation in gases: The absorption of CO and O_2," IEEE Transact. Ant. & Propagation, in preparation, 1987.

[22] Hill, R. J., "Absorption by the tails of the oxygen microwave resonances at atmospheric pressures," IEEE Transact. Ant. & Propagation, 35, 198-204, Feb. 1987.

[23] Rosenkranz, P. W., "Interference coefficients for overlapping oxygen lines in air," J. Quant. Spectr. Radiat. Transfer, in preparation, 1987.

[24] Fedoseev, L. I., and L. M. Koukin, "Comparison of the results of summer and winter measurements of atmospheric water vapor absorption at wavelengths 1.5 to 1.55 mm," Int. J. Infrared and Millimeter Waves, 5, 952-964, July 1984.

[25] Furashov, N. I., V. Y. Katkov, and V. Y. Ryadov, "On the anomalies of submillimeter absorption spectrum of atmospheric water vapor," Int. J. Infrared and Millimeter Waves, 5, 971-981, July 1984.

[26] Furashov, N. I., and V. Y. Katkov, "Humidity dependence of the atmospheric absorption coefficient in the transparency windows centered and 0.88 and 0.73 mm," Int. J. Infrared and Millimeter Waves, 6, 751-764, August 1985.

[27] Costales, J. B., G. F. Smoot, C. Witebsky, G. DeAmici, and S. D. Friedman, "Simultaneous measurements of atmospheric emissions at 10, 33, and 90 GHz," Radio Sci., 21, 47-55, Jan/Feb. 1986.

ACKNOWLEDGMENTS

The author wishes to thank D. H. Layton for his valuable contributions to the electronic design of the millimeter-wave spectrometer, J. P. Stricklen for his skillful programming efforts, and Ms. S. A. Kirby for the careful typing of this report.

APPENDIX

DRAFT (6/1/87) of invited contribution,

THE REFRACTIVE INDEX OF THE NEUTRAL ATMOSPHERE
FOR FREQUENCIES UP TO 1000 GHz

to

Landolt-Börnstein Handbook V.5.

Editors: W.Dieminger et al.,

Springer Verlag, Berlin-Heidelberg 1988:

"PHYSICS OF THE ATMOSPHERE"

Chapter 1.2.4.8

CONTENTS:

THE REFRACTIVE INDEX OF THE NEUTRAL ATMOSPHERE FOR FREQUENCIES UP TO 1000 GHZ

Hans J. Liebe
National Telecommunications and Information Administration,
Institute for Telecommunication Sciences, Boulder, CO

1. INTRODUCTION

Dry air and atmospheric water vapor are major millimeter-wave absorbers; so are suspended droplets (haze, fog, cloud) and precipitating water drops that emanate from the vapor phase. A practical model (designated program code: MPM) was formulated that simulates the refractive index $\underline{n} = n' - jn''$ of the atmospheric propagation medium for frequencies up to 1000 GHz (Liebe, 1985; Liebe, 1987). The main purpose of the program is to express the electromagnetic properties of the neutral atmosphere in terms of available and/or measurable quantities.

The free propagation of a plane electromagnetic wave at frequency f and an initial field strength E_0 in an isotropic gas medium over distance L is described by the complex transmission factor

$$\underline{\tau} = E(L)/E_0 = \exp[-(2\pi f/c)(n'' + jn')L]$$

where n'(f) and n"(f) are frequency-dependent measures of delay and loss, and c is the speed of light. Since the interaction with a neutral atmosphere is relatively weak, the refractive index is converted into a refractivity

$$\underline{N} = (\underline{n} - 1)10^6 \qquad \text{ppm},$$

in units of parts per million.

Refractivity N for moist air can be obtained, in principle, by a summation over all absorption features in a given volume element. In practice, various degrees of approximations are employed to reduce labor and computer time required, since the number of contributing spectral lines by the dominant absorbers (water vapor and oxygen) and by various trace gases (e.g., O_3) exceeds 10,000. The model MPM consists of local H_2O (30x) and O_2 (48x) lines below 1 THz and an empirical approximation to the contributions by H_2O lines above 1 THz. To complete the model, continuum spectra for dry air, suspended water droplets (haze, fog, cloud), and rain are added. The supporting

spectroscopic data base contains more than 450 coefficients.

1.1 Features of the Program MPM

A user-friendly parametric program was developed (see Section 2) that calculates the values of the complex refractivity

$$\underline{N} = N_0 + N'(f) + jN''(f) \qquad \text{ppm}$$

or corresponding path-specific quantities of particular interest to radio engineering; i.e.,

refractive delay	β_0	ns/km,
dispersive delay	$\beta(f)$	ps/km, and
attenuation	$\alpha(f)$	dB/km;

both sets for atmospheric conditions as a function of the variables f, P, T, RH, w_A (A/B/C/D), w, and R, as listed in the scheme below:

Variable	Symbol	Validity Range	Medium
frequency	f	≤ 1000 GHz	
barometric pressure	P	120-0 kPa	Moist
temperature	T	- 50- + 50°C	Air
relative humidity	RH	0-100%	
haze model: code A, B, C, D (or combinations thereof) plus hygroscopic aerosol reference concentration	w_A(80%RH)	RH=80-99.9% 0-1 mg/m^3	Haze
suspended water droplet concentration	w(100%RH)	0-10 g/m^3	Fog, Cloud
rain fall rate	R	0-200 mm/h	Rain

The height range 30 to 100 km is treated approximately excluding the detailed O_2-Zeeman effect and trace gas spectra (e.g., O_3, CO, N_2O, etc.), that are discussed in chapter 1.2.4.3. Program MPM is written with extensive comments to run on IBM-XT/AT + 8087 Coprocessor, or equivalent, micro computers.

1.2 Physical Variables

The purpose of this section is to relate measurable variables to N model-specific variables, whereby the state of dry air is described by a partial air pressure p in kPa, a relative inverse temperature variable is

$\theta = 300/(273.15 + T)$,

and relative humidity is given by

$$RH = (e/e_s)100 = (v/v_s)100 = 41.51(e/\theta^5)10^{(9.834\ \theta-10)} \leq 100\%. \qquad (1)$$

Equation (1) governs physical processes taking place in the atmosphere with respet to water vapor. Absolute (v) and relative (RH) humidity are inter-related through

$$v = (RH/5.752)\theta^6 10^{(10-9.834\ \theta)} = 7.271\ e\ \theta \quad g/m^3 \qquad (2)$$

where e is the partial water vapor pressure in kPa as part of the total (barometric) pressure $P = p + e$.

Water vapor variability at sea level (e.g., P = 101 kPa, $\theta = 1.016$ or 22°C) is typically:

	Dry	Normal	Humid	Saturated
v	1	10	17	$20 g/m^3$
RH	5	50	85	100 %

Suspended hydrometeors are described by the liquid water concentration w, which relates approximately to optical (0.55 μm) visibility U(km). A schematic categorization can be made by

	Haze	Fog	Stratus Cloud	Convective Cloud
$w \leq$	10^{-2}	10^{-1}	1	5 g/m^3
$U \geq$	1.1	0.27	0.07	0.03 km

Another atmospheric ingredient is hygroscopic aerosol with a mass concentration w_A in g/m^3. Solution droplets appear for RH > 80%, and haze conditions develop as RH approaches 100 percent. The growing haze droplets can reach values ($w < 0.1\ g/m^3$), sufficient to contribute to medium losses. Haze conditions are modeled by assuming that at the reference humidity, RH = 80%, the concentration $w_A(RH=80\%)$ is known. Any RH-dependent swelling/shrinking of w(RH) up to RH=99.9% is modeled by

$$w = w_A(C1-RH)/C2(100-RH) = w_A\ g(RH), \qquad (3)$$

where g(RH) is a growth function. The following values have been reported for C1, C2:

Case	Aerosol Species	C1	C2	g(RH=99.9%)
A	Rural	117	1.87	91
B	Urban	128	2.41	117
C	Maritime	183	5.31	162
D	C + Strong Wind (>10 km/h)	197	5.83	167

Average values of w_A for given stabilized climatic situations can be found in the literature. Typical values for w_A lie between 0.01 and 0.5 mg/m^3 and the increase to w can be substantial as indicated by the maximum prefog values g(99.9%).

Precipitation originates as a statistical event within clouds suspended in saturated air. Its vertical distribution is separated into two regions by the height of the 0°C isotherm, which can vary between ~6 km and ground level depending on season and latitude. The lower part is mostly liquid drops, and the upper region consists of frozen particles with occasional supercooled droplet-loadings by strong updrafts.

Point rain rates R have proven useful in modeling rain-induced $\underline{N}$ effects. Rain rate can be related to percent time t_R, a given value occurs over the period of an "average" year; to the effective rain cell extent L_R/L; and to the instaneous suspended liquid water concentration,

$$w_R = m \cdot R \qquad g/m^3.$$

In terms of these variables, a typical local rain may be classified as follows (horizontal path, L = 10 km):

	Drizzle	Steady	Heavy	Downpour	Cloudburst	
R	1	5	20	100	250	mm/h
t_R	2	0.5	0.07	0.001	0.0001	% per yr
L_R/L	1	1	0.7	0.35	0.2	
m	0.1	0.07	0.05	0.04	0.04	

The simple coefficient scheme reveals some fundamentals of rain. Changes in the factor m indicate rain rate-dependent characteristics of drop size distributions. Widespread steady rain occurs more uniformly and favors small drop sizes (≤1 mm diameter) which stay in the air longer. Heavy showers are more localized, favor larger drops and occur less frequently.

2. MODEL FOR COMPLEX REFRACTIVITY

The complex refractivity in N units (i.e., ppm = 10^{-6})

$$\underline{N}(f;P/T/RH,w_A/w,R) = N_o + N'(f) + jN''(f) \quad \text{ppm} \qquad (4)$$

is a macroscopic measure of interactions between radiation and absorbers. The refractivity consists of a frequency-independent term N_o plus various spectra of refractive dispersion N'(f) and absorption N"(f).

In radio engineering it is customary to express the imaginary part of (4) as power attenuation rate α and the real part as propagation delay rate β (with reference to vacuum) as follows:

$$\alpha = 0.1820\ f\ N''(f) \quad \text{dB/km} \qquad (5a)$$

and

$$\beta = 3.336[N_o + N'(f)] \quad \text{ps/km,} \qquad (5b)$$

where frequency f is in gigahertz (GHz) throughout.

Radio refractivity is defined to be $\underline{N} = N_o$ at f = 0 and consists of four terms; i.e.,

$$N_o = N_p^o + N_e^o + N_w^o + N_R^o.$$

The individual contributions are described for dry air by

$$N_p^o = 2.588\ p\ \theta, \qquad (6)$$

for water vapor by

$$N_e^o = 2.39\ e\ \theta + 41.6\ e\ \theta^2, \qquad (7)$$

for the SWD term N_w^o by (16c), and for the rain term N_R^o by (18c). The results (6) and (7) have been determined experimentally at microwave frequencies where dispersive contributions N(f) are negligible.

A calculation of the spectrum $\underline{N}(f)$ for frequencies up to 1000 GHz consists of several additive parts:

- Resonance information of n_a=48 oxygen lines and n_b=30 water vapor lines.
- Nonresonant O_2 and pressure-induced N_2 absorption ($\underline{N_D}$).
- Continuum absorption from far-wing contributions of strong H_2O lines falling in the frequency range 1-30 THz ($\underline{N_e}$).
- Suspended water droplet SWD term ($\underline{N_w}$).
- Rain-effect approximation($\underline{N_R}$).

Absorption and dispersion spectra are obtained from line-by-line calculations plus various continuum spectra $\underline{N}_{p,e,w,R}$ according to

$$N''(f) = \underbrace{\sum_{i=1}^{n_a} (SF'')_i}_{\text{Dry Air}} + N''_p + \underbrace{\sum_{i}^{n_b} (SF'')_i}_{\text{Water Vapor}} + N''_e + N''_w + \underbrace{N''_R}_{\text{SWD Rain}} \qquad (8a)$$

$$N'(f) = \sum_{i=1}^{n_a} (SF')_i + N'_p + \sum_{i}^{n_b} (SF')_i + N'_e + N'_w + N'_R \qquad (8b)$$

where S is the line strength in kilohertz, and F' and F" are real and imaginary parts of a line shape function in GHz^{-1}.

2.1 Local Line Absorption and Dispersion

The Van Vleck-Weisskopf function is modified to describe, to first order line overlap effects (Rosenkranz, 1987), which leads to local absorption and dispersion line profiles in the form

$$F''(f) = \left[\frac{1}{X} + \frac{1}{Y} - \frac{\delta}{\gamma}\left(\frac{\nu_o - f}{X} + \frac{\nu_o + f}{Y}\right)\right] A \qquad (9a)$$

and

$$F'(f) = \frac{Z - f}{X} + \frac{Z + f}{Y} - \frac{2}{\nu_o} + \delta\left(\frac{1}{X} - \frac{1}{Y}\right) A \qquad (9b)$$

with the abbreviations $A = \gamma f/\nu_o$,

$$X = (\nu_o - f)^2 + \gamma^2, \quad Y = (\nu_o + f)^2 + \gamma^2, \quad Z = (\nu_o^2 + \gamma^2)/\nu_o \ .$$

Standard line shapes F"(f), including the modified Van Vleck-Weisskopf function (9), predict in frequency regions of local line dominance about the same results for N"(f) as long as F"(f) exceeds by 0.1% the peak value at $f = \nu_o$. Far-wing contributions of smaller magnitude depend very much upon the chosen shape function. For $f \to \infty$, the wing response of (9a) becomes non-physical and is cut-off; i.e., F" = 0 when $(\nu_o + f) > 40\gamma$. So far, no line shape has been confirmed that predicts absorption intensities over ranges 10^{-3}

to $< 10^{-6}$ of $F''(\nu_o)$. Far-wing contributions from strong infrared water vapor lines, where $\alpha(\nu_o)$ can exceed 10^6 dB/km, are accounted for summarily by empirical correction [see (15a)].

The line parameters are calculated by the expressions below:

Symbol	O_2 Lines in Air	H_2O Lines in Air	Eq.
S, kHz	$a_1 p\ \theta^3 \exp[a_2(1-\theta)]$	$b_1 e\ \theta^{3.5} \exp[b_2(1-\theta)]$	(10)
γ, GHz	$a_3(p\theta^{(0.8-a_4)} + 1.1e\theta)$	$b_3(p\theta^{0.6} + 4.80e\theta^{1.1})$	(11)
δ	$a_5 p\ \theta^{a_6}$	0	(12)

Line center frequencies ν_o and the spectroscopic coefficients $a_1(\geq 10^{-7}$ Hz/Pa) to a_6 and $b_1(\geq 10^{-3}$ Hz/Pa) to b_3 for strength S, width γ, and overlap correction δ are listed in the Line Data File of MPM (see part 3: CD-ROM).

For the O_2 lines in air, equations (9) to (12) are valid for altitudes $h \leq 35$km ($p > 0.7$ kPa), where lines are pressure-broadened. Higher up, Zeeman-splitting and Doppler-broadening of the Zeeman components must be taken into account (Liebe and Gimmestad, 1978). An estimate for $h > 35$ km is made by geometrically adding to the pressure proportional width γ_a in (11) a second term

$$\gamma_h = \left[\gamma_a^2 + (25H)^2\right]^{0.5} \quad \text{GHz} \qquad (11a)$$

where H is the scalar earth magnetic field strength in Tesla, ranging from 0.2 to 0.9×10^{-4}. The O_2 spectrum vanishes around $H \approx 90$ km.

For the H_2O lines in air Doppler-broadening has to be considered at altitudes above 60 km ($p < 0.07$ kPa). An approximation is made by replacing the width γ_b in (11) with

$$\gamma_h = (\gamma_b^2 + \gamma_D^2)^{0.5} \quad \text{GHz} \qquad (11b)$$

where $\gamma_D^2 = 2.14\nu_o^2 \times 10^{-12}/\theta$ is the squared Doppler width. In applications requiring the detailed mesospheric line shape it is necessary to apply the more correct Voigt line shape.

2.2 Continuum Spectra for Air

Continuum spectra in (8) identify dry air and water vapor terms $\underline{N_p} + \underline{N_e}$ and must be added to the selected group of local (MPM) O_2 and H_2O resonance lines described by (9). Continuum absorption increases montonically with frequency.

The dry air continuum

$$N''_p(f) = f\left(2a_o\{\gamma_o[1 + (f/\gamma_o)^2]\}^{-1} + a_p p\,\theta^{1.5}\right) p\theta^2 \qquad (13a)$$

and

$$N'_p(f) = a_o\{[1 + (f/\gamma_o)^2]^{-1} - 1\}\, p\,\theta^2 \qquad (13b)$$

make a small contribution at ground level pressures due to the nonresonant O_2 spectrum below 10 GHz, and a pressure-induced N_2 spectrum that is effective above 100 GHz. A width parameter for the Debye spectrum of O_2 is formulated in accordance with (11) to be $\gamma_o = 4.8 \times 10^{-3}(p + 1.1e)\theta^{0.8}$(GHz) (Rosenkranz, 1987). The continuum coefficients are $a_o = 3.07 \times 10^{-4}$ and $a_p = 1.40(1\text{-}1.2\ f^{1.5}10^{-5})10^{-10}$.

Water vapor continuum absorption has been a major source of uncertainty in predicting millimeter wave attenuation rates, especially in the window ranges. Moist air attenuation α at a frequency that falls within a window can be expressed by

$$\alpha = k_s(T)e^2 + k_f(T)e\,p + k_d(T)p^2 \,. \qquad (14)$$

A series of controlled laboratory measurements was performed at 137.8 GHz to determine the k-coefficients. Data $\alpha(T,e,p)$ were taken covering the following range of parameters:

temperature	T = 8 to 43° C
vapor pressure	e = 0 to e_1(RH ≤ 95%) and
total pressure	P = e_1 + p, where p = 0 to 150 kPa.

Experimental data were reduced to a reference temperature T_o = 26.85° C (θ = 1). The temperature dependence of each k-coefficient ($k_{s,f,d}$) was fitted to a power law $k(T) = k\theta^x$. Moist air attenuation at f_x = 137.8 GHz behaved as follows:

$$k_s = 0.133(4)\theta^{10.3(3)}, \quad k_f = 5.68(5)10^{-3}\theta^{3.0(4)}, \quad k_d = 2(1)10^{-6}\theta^3. \quad (14a)$$

Values in parentheses give the standard deviation from the mean in terms of final listed digits. The experimental results (14), containing foremost contributions from water vapor continuum absorption, were used to "calibrate" the program MPM by enforcing agreement between experimental and predicted data; further, an f^2 dependence was assumed.

The water vapor continuum is derived from fitting experimental data (14) in the case of

$$N_e''(f) = f(b_f p + b_e e)e\ \theta^3 \quad (15a)$$

and based on theoretical data in the case of

$$N_e'(f) = f^2 b_o e\ \theta^3 \ , \quad (15b)$$

where (Liebe, 1987)

$$b_f = 1.13 \times 10^{-6},$$
$$b_e = 3.57 \times 10^{-5}\theta^{7.5}, \text{ and}$$
$$b_o = 6.47 \times 10^{-6} .$$

In summary:
Equation (15) is needed to supplement local line (MPM) contributions, the coefficient b_f is valid only for the selected local line base treated with line shape (9), and the strong self-broadening component $b_e e^2$ is nearly unaffected by (9). The coefficient b_o and both exponents in (15b) were obtained by fitting dispersion results of line-by-line calculations for the rotational H_2O spectrum above 1 THz.

2.3 Suspended Water Droplet Continuum (Haze, Fog, Cloud)

Suspended water droplets (SWD) in haze, fog, or clouds are millimeter wave absorbers. Their size range of radii is below 50 μm, which allows the Rayleigh approximation of Mie scattering theory to be used for calculating refractivity contributions N_w to (8) in the form

$$N_w''(f) = (9/2)w/\varepsilon''(1 + \eta^2), \quad (16a)$$

$$N_w'(f) = (9/2)w\ [1/(\varepsilon_o + 2) - \eta/\varepsilon''(1 + \eta^2)], \quad (16b)$$

and

$$N_w^o = (3/2)w\,[1 - 3/(\varepsilon_o + 2)], \qquad (16c)$$

where $\eta = (2 + \varepsilon')/\varepsilon''$; ε', ε'' are real and imaginary, and ε_o static parts of the permittivity for water. The contribution of (16c) is added to equation (6).

Values for the dielectric spectra $\underline{\varepsilon}(f)$ of water are calculated with a new double-Debye model (Manabe et al., 1987):

$$\varepsilon'(f) = \varepsilon_2 + (\varepsilon_o - \varepsilon_1)/[1 + (f/f_D)^2] + (\varepsilon_1 - \varepsilon_2)/[1 + (f/f_S)^2], \qquad (17a)$$

$$\varepsilon''(f) = f\left\{(\varepsilon_o - \varepsilon_1)/f_D[1 + (f/f_D)^2] + (\varepsilon_1 - \varepsilon_2)/f_S[1 + (f/f_S)^2]\right\}, \qquad (17b)$$

$$\varepsilon_o = 77.66 + 103.3(\theta - 1), \qquad (17c)$$

where $\varepsilon_1 = 5.48$, $\varepsilon_2 = 3.51$,

$f_D = 20.09 - 142(\theta - 1) + 294(\theta - 1)^2$ GHz, and
$f_S = 590 - 1500(\theta - 1)$ GHz.

Equation (17) is valid for frequencies up to 1000 GHz over a temperature range from -10 to +30° C.

2.4 Rain Effects

The refractivity of rain is identified in (8) by $\underline{N}_R = N_R' + jN_R''$. Drop diameters (0.1 - 6 mm) and millimeter wavelengths are comparable, thus causing appreciable interactions due to Mie absorption and scattering. Bypassing elaborate, lengthy Mie calculations which require drop shape and size distributions as well as the complex dielectric properties of water (17), rain refractivity spectra are approximated via

$$N_R''(f) = aR^b \qquad (18a)$$

$$N_R'(f) = 70R[1/(f_R^2 + f^2) - 1/f_R^2] \qquad (18b)$$

$$N_R^o = 70R/f_R^2 \qquad (18c)$$

where $f_R = (52 - 0.22R)$ GHz. Frequency-dependent coefficient a and exponent b were calculated using dropsize spectra of Laws and Parsons and a temperature of T = 0° C. A regression fit to individual (a,b)-pairs over the frequency range from 1 to 1000 GHz resulted in the following calculation scheme:

$a = x_1 f^{x_2}$			$b = x_3 f^{x_4}$		
f	x_1	x_2	f	x_3	x_4
GHz			GHz		
1 to 2.9	3.51×10^{-4}	1.03	1 to 8.5	0.851	0.158
2.9 to 54	2.31×10^{-4}	1.42	8.5 to 25	1.41	-0.0779
54 to 180	0.225	-0.301	25 to 164	2.63	-0.272
180 to 1000	18.6	-1.151	164 to 1000	0.616	0.0126

3. CONCLUSIONS

The parametric model MPM for atmospheric refractivity

$$\underline{N}(f,P/T/RH,\ w_A/w,R)$$

was developed for applications in areas such as telecommunications, remote sensing, and radio astronomy. Details of its structure and operation are explained in the extensive COMMENTS part of the code, that is available under MPM in part 3: CD-ROM. The memory capacity required for MPM is 355 kbytes.

The format of the numerical print-out is demonstrated by the identical example given in TABLE 1 for the $\underline{N}$ version [see (4)] and in TABLE 2 for the α/β version [see (5)]. A plotting system at the user's choice (e.g., HALO) can be added to include features such as auto or manual scaling, multiple cases (e.g., 9 curves with up to 500 points each), special labels, etc. An example of a graphical presentation for a sea level condition of moist air ($w_A = w = R = 0$) exhibits spectra at various relative humidities (RH = 0-100%) for the $\underline{N}$ version in FIGURE 1 and for the identical case as α/β version in FIGURE 2.

Acknowledgements

The author wishes to thank J. P. Stricklen for his skillful programming efforts. The work was supported in part by the Naval Ocean Systems Center (Ref: RA35 G80), and the experimental portion by the U. S. Army Research Office under Contract ARO 107-86.

REFERENCES for 1.2.4.8:

(detailed references are given in the COMMENTS part of MPM in part 3: CD-ROM)

Liebe, H. J., Gimmestad, G. G.: Radio Sci. 13 (1978) 245.

Liebe, H. J.: Radio Sci. 20 (1985) 1069.

Liebe, H. J.: FREQUENZ 41 (1987) 31.

Manabe, T., Liebe, H. J., Hufford, G. H.: IEEE Trans. AP, in preparation.

Rosenkranz, P. W.: J. Quant. Spectr. Rad. Transf., " " .

TABLE 1.

FREQUENCY PROFILES OF ATMOSPHERIC COMPLEX REFRACTIVITY

INPUT Valid Parameter ranges indicated by [ ]):

CASE	PRES.,P (kPa)	TEMP.,T (C)	REL. HUM.,RH (%)	HAZE MODEL (mg/m3)	SUSP. DROP.,w (g/m3)	RAIN RATE,R (mm/hr)
[1-9]	[0 -110]	[+/-50]	[0-100]	[0-1]	[0-10]	[0-200]
1	101.3	15.0	100.0	: 0.00	1.000	10.0

Minimum Frequency F1 0.000 (GHz)
Maximum Frequency F2 [1000.]1000.000 (GHz)
Frequency Step [max 500] dF 100.000 (GHz)

OUTPUT:
Case Number: 1 (No = 351.18 ppm)

MOIST AIR (v= 12.81 g/m3)

FREQUENCY (GHz)	DRY AIR +	WATER VAPOR +	HAZE, FOG CLOUD +	RAIN	= TOTAL
	N"-IMAGINARY PART (ppm)				
	N'-REAL PART (ppm)				
0.000	+++++++++	+++++++++	+++++++++	+++++++++	+++++++++
	0.220E-09	-.317E-07	0.278E-08	0.431E-08	-.244E-07
100.000	0.168E-02	0.454E-01	0.242E+00	0.317E+00	0.607E+00
	-.219E+00	0.321E+00	-.139E+00	-.226E+00	-.264E+00
200.000	0.476E-03	0.149E+00	0.288E+00	0.190E+00	0.629E+00
	-.170E+00	0.107E+01	-.299E+00	-.266E+00	0.334E+00
300.000	0.561E-03	0.174E+00	0.284E+00	0.120E+00	0.579E+00
	-.162E+00	0.352E+01	-.391E+00	-.275E+00	0.269E+01
400.000	0.807E-03	0.481E+00	0.276E+00	0.869E-01	0.845E+00
	-.157E+00	0.619E+01	-.450E+00	-.278E+00	0.530E+01
500.000	0.104E-02	0.118E+01	0.268E+00	0.675E-01	0.152E+01
	-.162E+00	0.192E+02	-.495E+00	-.279E+00	0.183E+02
600.000	0.846E-03	0.225E+01	0.260E+00	0.549E-01	0.257E+01
	-.159E+00	-.172E+02	-.532E+00	-.280E+00	-.182E+02
700.000	0.977E-03	0.101E+01	0.252E+00	0.461E-01	0.131E+01
	-.157E+00	0.687E+01	-.563E+00	-.281E+00	0.587E+01
800.000	0.117E-02	0.112E+01	0.242E+00	0.396E-01	0.140E+01
	-.161E+00	-.635E+01	-.589E+00	-.281E+00	-.738E+01
900.000	0.101E-02	0.795E+00	0.232E+00	0.347E-01	0.106E+01
	-.159E+00	0.716E+01	-.611E+00	-.281E+00	0.611E+01
1000.000	0.103E-02	0.603E+01	0.223E+00	0.308E-01	0.628E+01
	-.159E+00	-.134E+02	-.629E+00	-.282E+00	-.145E+02

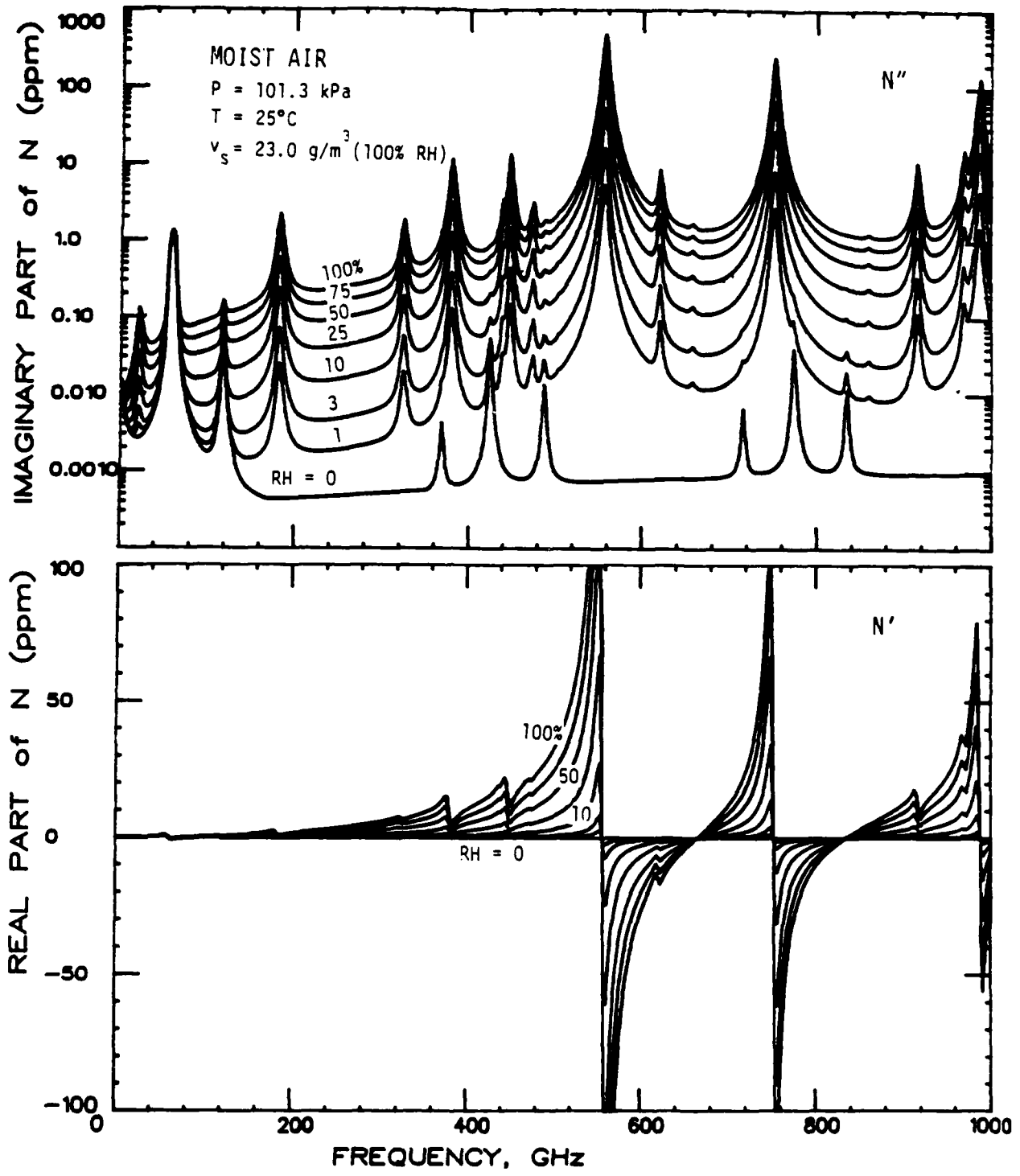

Figure A1.

Moist air refractivity $\underline{N}$ = N' + jN" for a sea level condition (P,T) and various relative humidities (RH) over the frequency range from 0 to 1000 GHz.

TABLE 2.

FREQUENCY PROFILES OF ATTENUATION AND DELAY RATES

INPUT Valid Parameter ranges indicated by [ ]):

CASE [1-9]	PRES.,P (kPa) [0 -110]	TEMP.,T (C) [+/-50]	REL. HUM.,RH (%) [0-100]	HAZE MODEL (mg/m3) [0-1]	SUSP. DROP.,w (g/m3) [0-10]	RAIN RATE,R (mm/hr) [0-200]
1	101.3	15.0	100.0	: 0.00	1.000	10.0

Minimum Frequency F1 0.000 (GHz)
Maximum Frequency F2 [1000.]1000.000 (GHz)
Frequency Step [max 500] dF 100.000 (GHz)

OUTPUT:
Case Number: 1 (Refractive delay = 1171.5 ps/km)

	MOIST AIR (v= 12.81 g/m3)				
	DRY AIR	+ WATER VAPOR	+ HAZE, FOG CLOUD	+ RAIN	= TOTAL
FREQUENCY	α-ATTENUATION (dB/km)				
(GHz)	β-DISPERSIVE DELAY (ps/km)				
0.000	0.00	0.00	0.00	0.00	0.00
	0.00	0.00	0.00	0.00	0.00
100.000	0.03	0.83	4.41	5.78	11.05
	-0.73	1.07	-0.46	-0.75	-0.88
200.000	0.02	5.44	10.50	6.93	22.88
	-0.57	3.56	-1.00	-0.89	1.11
300.000	0.03	9.50	15.52	6.57	31.62
	-0.54	11.75	-1.30	-0.92	8.99
400.000	0.06	35.02	20.11	6.32	61.51
	-0.52	20.64	-1.50	-0.93	17.68
500.000	0.09	107.25	24.43	6.14	137.92
	-0.54	64.18	-1.65	-0.93	61.06
600.000	0.09	246.00	28.44	6.00	280.53
	-0.53	-57.35	-1.77	-0.94	-60.59
700.000	0.12	128.84	32.07	5.87	166.91
	-0.52	22.92	-1.88	-0.94	19.58
800.000	0.17	162.65	35.28	5.77	203.87
	-0.54	-21.20	-1.96	-0.94	-24.63
900.000	0.17	130.27	38.08	5.68	174.20
	-0.53	23.88	-2.04	-0.94	20.37
1000.000	0.19	1097.36	40.50	5.61	1143.65
	-0.53	-44.84	-2.10	-0.94	-48.40

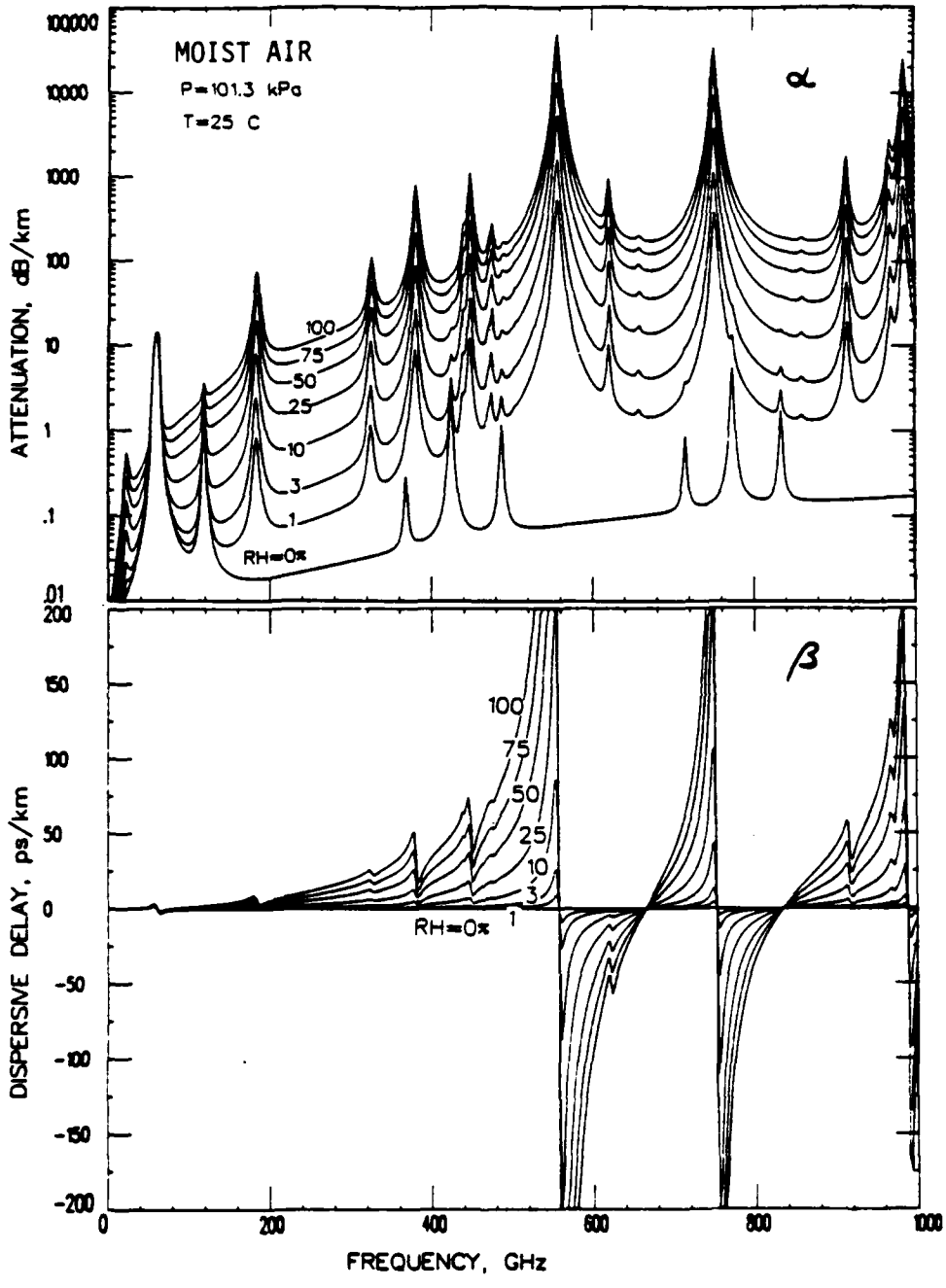

Figure A2. Moist air attenuation (α) and delay (β) rates for a sea level condition (P,T) and various relative humidities (RH) over the frequency range from 1 to 1000 GHz.

END

10-87

DTIC